

**A novel role of B-RAF in the regulation of ion channels  
and transporters**

**Inaugural-Dissertation  
zur Erlangung des Doktorgrades  
der Humanwissenschaften**

**der Medizinischen Fakultät  
der Eberhard Karls Universität  
zu Tübingen**

**vorgelegt von**

**Tatsiana Castor (geb. Pakladok)**

**aus**

**Erchi, Weißrussland**

**2016**

Dekan:

Professor Dr. I. B. Autenrieth

1. Berichterstatter:

Professor Dr. F. Lang

2. Berichterstatter:

Professor Dr. R. Feil

3. Berichterstatter:

Professor Dr. A. Schwab

# Contents

<b>CONTENTS.....</b>	<b>3</b>
<b>ABBREVIATIONS.....</b>	<b>6</b>
<b>1 INTRODUCTION .....</b>	<b>8</b>
<b>1.1 RAF proteins.....</b>	<b>8</b>
1.1.1 The structure of B-RAF .....	8
1.1.2 B-RAF activation .....	9
1.1.3 The role of B-RAF .....	9
1.1.4 B-RAF in the oncogenesis .....	11
1.1.5 B-RAF and the membrane transport regulation.....	12
<b>1.2 Ion channels .....</b>	<b>12</b>
1.2.1 The potassium ion channels .....	12
1.2.2 hERG K <sup>+</sup> channels .....	13
1.2.3 hERG and the Long QT syndrome type 2 (LQT2) .....	14
1.2.4 Other hERG channelopathies .....	15
1.2.5 hERG in cancer.....	16
<b>1.3 Carrier proteins .....</b>	<b>16</b>
1.3.1 The sodium-glucose cotransporter SGLT1 .....	16
1.3.2 The sodium-coupled phosphate cotransporters NaPi-IIa and NaPi-IIb .....	17
<b>1.4 Aim of the study .....</b>	<b>21</b>
<b>2 MATERIALS AND METHODS .....</b>	<b>22</b>
<b>2.1 Constructs and cRNA synthesis .....</b>	<b>22</b>
<b>2.2 Agarose gel electrophoresis .....</b>	<b>24</b>
<b>2.3 Heterologous expression of the ion channels and transporters in <i>Xenopus laevis</i> oocytes.....</b>	<b>25</b>
<b>2.4 <i>Xenopus laevis</i> oocytes preparation and maintenance.....</b>	<b>25</b>

<b>2.5</b>	<b>cRNA injection</b> .....	<b>26</b>
<b>2.6</b>	<b>Electrophysiological measurements</b> .....	<b>27</b>
<b>2.7</b>	<b>Whole-cell patch clamp</b> .....	<b>29</b>
<b>2.8</b>	<b>Flow cytometry</b> .....	<b>29</b>
<b>2.9</b>	<b>Biotinylation of cell surface proteins</b> .....	<b>30</b>
<b>2.10</b>	<b>Western blotting</b> .....	<b>31</b>
2.10.1	The SDS polyacrylamide gel electrophoresis (SDS-PAGE) .....	31
2.10.2	Protein transfer to a membrane and protein detection .....	32
<b>2.11</b>	<b>Detection of cell surface protein expression by chemiluminescence</b> .....	<b>33</b>
<b>2.12</b>	<b>Immunocytochemistry and confocal microscopy</b> .....	<b>34</b>
<b>2.13</b>	<b>Cell culture</b> .....	<b>36</b>
<b>2.14</b>	<b>Data analysis</b> .....	<b>37</b>
<b>3</b>	<b>RESULTS</b> .....	<b>38</b>
<b>3.1</b>	<b>B-RAF regulates hERG channels</b> .....	<b>38</b>
3.1.1	Wild-type B-RAF stimulates the hERG-mediated current in <i>Xenopus</i> oocytes .....	38
3.1.2	The current-voltage relationship of hERG currents with or without co-expression of wild-type B-RAF.....	39
3.1.3	Co-expression of wild-type B-RAF increases the hERG-HA protein abundance in the cell membrane .....	40
3.1.4	Effect of the B-RAF inhibitor PLX-4720 on the hERG-mediated current.....	41
3.1.5	Effect of the B-RAF inhibitor PLX-4720 on the hERG-HA cell surface protein abundance in <i>Xenopus</i> oocytes .....	42
3.1.6	Effect of the B-RAF inhibitor PLX-4720 on the hERG cell membrane protein abundance in rhabdomyosarcoma RD cells .....	42
3.1.7	B-RAF inhibitor PLX-4720 decreases hERG cell membrane protein abundance in rhabdomyosarcoma RD cells .....	43
3.1.8	B-RAF inhibitor PLX-4720 decreases the hERG-mediated tail currents in rhabdomyosarcoma RD cells .....	44
<b>3.2</b>	<b>B-RAF regulates the sodium-coupled glucose transporter SGLT1</b> .....	<b>45</b>

3.2.1	Wild-type B-RAF stimulates the SGLT1 mediated electrogenic glucose transport ...	45
3.2.2	B-RAF enhanced the maximal current.....	46
3.2.3	B-RAF increases the SGLT1 protein abundance in the cell membrane.....	47
<b>3.3</b>	<b>B-RAF regulates the sodium-coupled phosphate cotransporters NaPi-IIa and NaPi-IIb.....</b>	<b>49</b>
3.3.1	Wild-type B-RAF increased the electrogenic phosphate transport in NaPi-IIa-expressing <i>Xenopus</i> oocytes .....	49
3.3.2	Wild-type B-RAF increased the maximal phosphate transport rate in the NaPi-IIa-expressing <i>Xenopus</i> oocytes .....	50
3.3.3	Wild-type B-RAF increased the NaPi-IIa protein abundance at the cell membrane of <i>Xenopus</i> oocytes.....	51
3.3.4	Effect of the B-RAF inhibitor PLX-4720 on NaPi-IIa protein abundance at the cell surface in HEK293 cells .....	52
3.3.5	Wild-type B-RAF increased the electrogenic phosphate transport in NaPi-IIb-expressing <i>Xenopus</i> oocytes .....	53
3.3.6	Wild-type B-RAF increased the maximal phosphate transport rate in NaPi-IIb-expressing <i>Xenopus</i> oocytes .....	54
<b>4</b>	<b>DISCUSSION .....</b>	<b>55</b>
<b>5</b>	<b>SUMMARY .....</b>	<b>60</b>
<b>6</b>	<b>REFERENCES .....</b>	<b>64</b>
<b>7</b>	<b>CONTRIBUTION .....</b>	<b>76</b>
<b>8</b>	<b>ORIGINAL PAPERS.....</b>	<b>77</b>
<b>9</b>	<b>ACKNOWLEDGMENTS.....</b>	<b>78</b>
<b>10</b>	<b>CURRICULUM VITAE .....</b>	<b>79</b>

## Abbreviations

aLQTS	Acquired long QT syndrome
ATP	Adenosine triphosphate
Bcl-2	B-cell lymphoma 2
BSA	Bovine serum albumin
cDNA	Complementary DNA
cNBD	Cyclic nucleotide binding domain
CR	Conserved region
CRD	Cysteine-rich domain
cRNA	Complementary RNA
C-terminus	COOH-terminal domain
ddH <sub>2</sub> O	Double-distilled water
DEPC	Diethylpyrocarbonate
DNA	Deoxyribonucleic acid
E. coli	<i>Escherichia coli</i>
EAG	Ether-a-go-go
EDTA	Ethylenediaminetetraacetic acid
EGFR	Epidermal growth factor receptor
ELISA	Enzyme-linked immunosorbent assay
ERK	Extracellular signal-regulated kinase
FGF23	Fibroblast growth factor 23
FITC	Fluorescein isothiocyanate
GLUT1	Glucose transporter 1
GTP	Guanosine-5'-triphosphate
GTPase	Guanosine-5'-triphosphatase
HEK293 cells	Human embryonic kidney 293 cells
hERG	Human <i>ether-a-go-go</i> related gene
hERG-HA	hERG containing an extracellular hemagglutinin epitope
HRP	Horseradish peroxidase
IGF	Insulin-like growth factor
IGF1	Insulin-like growth factor 1
IgG	Immunoglobulin G
K <sub>2P</sub>	Two-pore domain potassium channels
K <sub>Ca</sub>	Calcium-activated potassium channels
<i>KCNH2</i>	Human <i>ether-a-go-go</i> related gene
KD	Kinase domain
K <sub>ir</sub>	Inwardly rectifying potassium channels
K <sub>m</sub>	The Michaelis constant
K <sub>v</sub>	Voltage-gated potassium channels
K <sub>v</sub> 11.1	11 <sup>th</sup> member of the voltage-gated potassium channel family
LB agar	Lysogeny broth agar
LB medium	Lysogeny broth medium
LQT2	Long QT syndrome type 2

LQTS	Long QT syndrome
MAP	Mitogen-activated protein
MAPK	Mitogen-activated protein kinase
MAPK pathway	Mitogen-activated protein kinase pathway
MAPKK	Mitogen-activated protein kinase kinase
MAPKKK	Mitogen-activated protein kinase kinase kinase
MEK	Mitogen/extracellular signal-regulated kinase
NaPi-IIa	Na <sup>+</sup> /phosphate cotransporter IIa
NaPi-IIb	Na <sup>+</sup> /phosphate cotransporter IIb
NHE1	Sodium proton exchanger isoform 1
NIS	Sodium/Iodide symporter
N-terminus	NH <sub>2</sub> -terminal domain
PAS domain	Per (period circadian protein)-Arnt (aryl hydrocarbon receptor nuclear translocator protein)-Sim (single-minded protein) domain
PBS	Phosphate-buffered saline
P <sub>i</sub>	Phosphate
PVDF membrane	Polyvinylidene fluoride membrane
RAF	Rapidly accelerated fibrosarcoma
RAS	Rat sarcoma
RBD	RAS-binding domain
RD cells	Rhabdomyosarcoma cells
RNA	Ribonucleic acid
RNase	Ribonuclease
rNTPs	Ribonucleoside triphosphates
SDS	Sodium dodecyl sulfate
SEM	Standard error of the mean
SGLT1	Sodium-dependent glucose cotransporter member 1
SLC34 family	Solute carrier family 34
SLC34A1	Solute carrier family 34 member 1
SLC34A2	Solute carrier family 34 member 2
SLC5	The sodium/glucose cotransporter family
SLC5A1	Sodium/glucose cotransporter 1
TAE buffer	Tris-acetate-EDTA buffer
TBS	Tris-buffered saline
TBST	Tris-buffered saline and Tween 20
TEVC	Two-electrode voltage clamp technique
UV	Ultraviolet
VGK	Voltage-gated potassium channel
VSD	Voltage sensor domain

# 1 Introduction

## 1.1 RAF proteins

RAF proteins, named for Rapidly Accelerated Fibrosarcoma, are effectors of the receptor tyrosine kinase and were discovered as a retroviral oncogene (1, 2). There are three known mammalian RAF isoforms: A-RAF, B-RAF and C-RAF. All three isoforms are ubiquitously expressed, although there are significant differences in the expression levels depending on the tissue type (3). The RAF kinases are direct effectors of RAS. B-RAF is a serine/threonine protein kinase, an important component of the RAS/RAF/MEK/ERK mitogen-activated protein kinase (MAPK) pathway. In this cascade, B-RAF functions as a mitogen-activated protein (MAP) kinase kinase kinase (MAPKKK).

### 1.1.1 The structure of B-RAF

B-RAF consists of three conserved regions (CR<sub>s</sub>) (Figure 1). CR1 and CR2 are located at the N-terminus of the protein. These domains have a negative regulatory role in the RAF activation (4). The CR1 domain contains a RAS-binding domain (RBD) and a cysteine-rich domain (CRD). The RBD and CRD are involved in the interaction with the activated small GTPase RAS. The CRD also binds the membrane phospholipid, phosphatidylserine (5). The CR2 contains phosphorylation sites, participating in the RAF activation (6). The CR3 is located in the C-terminus of the protein and contains the kinase domain (KD). The catalytic domain CR3 contains two folding domains with an adenosine triphosphate (ATP)-binding site and a regulatory activating loop at the mouth of the active side (7). The N-terminal regulatory domain controls the activity of the kinase domain and its removal results in the constitutive oncogenic activation (6).



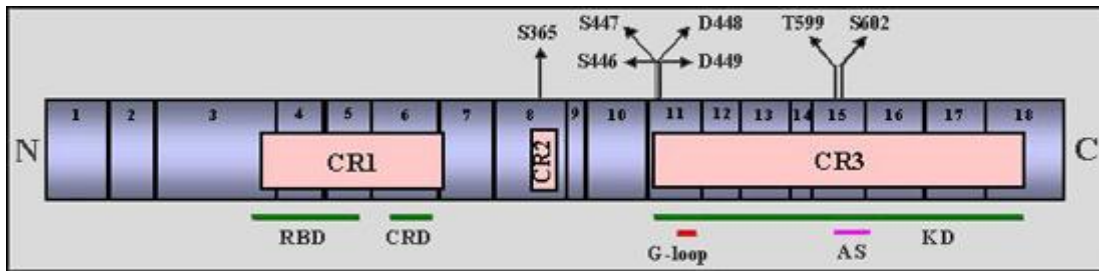


**Figure 1:** Structure and regulatory phosphorylation sites of B-RAF (8)

### 1.1.2 B-RAF activation

In the absence of stimuli, B-RAF adopts a closed conformation, where the N-terminus inhibits the catalytic C-terminus (9). This inactive conformation is stabilized through the phosphorylation of S365 residue (10). When this residue is dephosphorylated, the adaptor protein 14-3-3 is displaced from CR2 and B-RAF is activated (6). Another critical step in the B-RAF activation is an interaction of the RAS-binding domain of B-RAF and the GTP-bound RAS (11). This recruits B-RAF to the cell membrane from the cytosol and induces an open conformation which disrupts autoinhibitory interactions (12, 13). The N-region of B-RAF is permanently negatively charged due to the presence of aspartate at the position DD448/9 and the constitutive phosphorylation of S446 (14). This charged N-terminus of B-RAF is, at least partly, responsible for the higher basal *in vitro* kinase activity compared to A-RAF and C-RAF.

The activity of B-RAF also depends on the formation of homo- and heterodimers (15). It was shown that B-RAF and C-RAF heterodimerize in multiple cell lines in response to mitogens (16). 14-3-3 protein crosslinks these RAF isoforms by binding to the C-terminal sites on each kinase (16).

### 1.1.3 The role of B-RAF

B-RAF is expressed in a wide range of tissues, however the highest expression levels are observed in neuronal tissues and testis, hematopoietic cells, fetal brain and the adult cerebrum (17).

Most of the studies focused on the functional role of B-RAF in cancer. These data were mainly obtained using cell culture models, which have several limita-

tions. The further understanding of the biological role of this kinase comes from knockout and transgenic animal models.

Several studies indicate an essential role of B-RAF in the embryonic development (18-20). It was shown, that this kinase has a specific function in mediating the survival of sensory and motoneurons during the development (18). B-RAF knockout mice die of vascular defects caused by the death of endothelial cells during the midgestation (19, 20). These data show that B-RAF is a critical signalling factor in the formation of the vascular system as well as its involvement in the programmed cell death (19).

The RAF proteins and the MAPK pathway have shown to play the key role in various physiological processes such as cell proliferation, cell differentiation, apoptosis and cell cycle progression (21-23).

Figure 2 illustrates the simplified RAF/MEK/ERK cascade. It was shown, that B-RAF can phosphorylate and activate MAPKKs (MAP kinase kinases) which are called MEKs (MAPK or ERK kinases). MEKs in turn phosphorylate and activate MAPKs (MAP kinases) called ERKs (extracellular signal-regulated kinases). Activated ERKs can translocate into the nucleus where they phosphorylate transcription factors, by that regulating their activity (24).

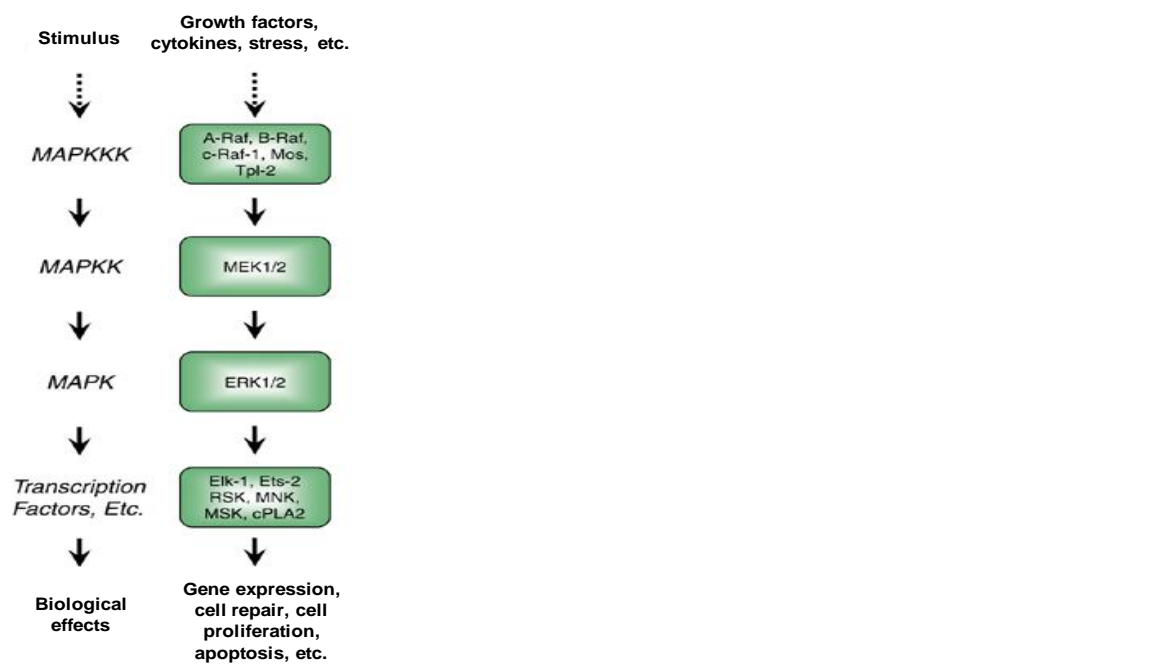


**Figure 2:** The RAF/MEK/ERK cascade (modified from Roberts & Der, 2007) (25)

This pathway can be activated by IGF, which plays an important role in the proliferation of various cell types, in the growth and development of multiple tumours (26). It has been shown that IGF is a potent mitogen and antiapoptotic factor for a variety of cells (27).

The RAS/RAF/MEK/ERK signalling pathway is an attractive target for the treatment of numerous cancers. During the last years, several selective RAF and MEK small molecule inhibitors have been tested in phase I and phase II of clinical trials (28). Other approaches in the treatment of cancer are targeting the expression of RAF, using RNA interference and antisense RNA molecules, as well as targeting the RAS-RAF interaction (29).

#### **1.1.4 B-RAF in the oncogenesis**

The importance of B-RAF in the oncogenesis was shown by the finding that it is mutated in approximately 7% of human cancers with the highest frequencies in malignant melanoma (60-70%), thyroid (30-50%), ovarian (approximately 30%), colorectal carcinomas (5-20%) and 1-3% in a wide variety of other cancers (30). Interestingly, the most of these mutations occur in the kinase domain, usually resulting in an elevated kinase activity which leads to the constitutive activation of the ERK pathway (31). A single substitution of glutamate to valine at residue 600 (formally labelled as V599E) accounts for 90% of the B-RAF mutations (32).

Taking into consideration the significance of B-RAF in the tumourigenesis, the inhibitors targeting this kinase and, in particular, the oncogenic form of B-RAF became particular important for the cancer therapy. Some of them were approved for clinical studies and show promising therapeutic effects. They inhibit the RAF/MEK/ERK pathway as well as tumour angiogenesis and induce tumour cell apoptosis. Among them are vemurafenib, sorafenib and PLX-4720 (33).

However, the effectiveness of the inhibitors is limited by the emergence of drug resistance. Furthermore, a series of side effects were observed in the patients, treated with B-RAF inhibitors. Therefore, the development of new inhibitors as well as combinational treatments that delay or prevent the drug-resistance is required (34).

### **1.1.5 B-RAF and the membrane transport regulation**

Only a limited number of the published data indicates the involvement of B-RAF in the regulation of the cell membrane transport. Karki et al. have shown that this kinase simulates the activity of the sodium proton exchanger isoforms 1 (NHE1) (35). NHE1 is a plasma membrane protein, which is ubiquitously expressed and responsible for the intracellular pH regulation, cell migration, cell volume and proliferation (35). B-RAF stimulates the activity of the exchanger by binding to the cytosolic regulatory tail. However, the nature of this complex still needs to be identified.

In another study, the association of the common B-RAF mutation V600E and the overexpression of the glucose transporter 1 (GLUT1) was shown (36). In papillary thyroid carcinoma this association leads to an increased cells proliferation.

Yun et al. reported that in the colorectal cancer cell lines with mutated B-RAF the expression of GLUT1 is also upregulated. The mutant cells exhibited an enhanced glucose uptake and survived in low glucose conditions (37).

There have been several studies which showed that B-RAF V600E induced suppression of the sodium/iodide symporter (NIS) in papillary thyroid carcinoma (38-40).

## **1.2 Ion channels**

Ion channels are transmembrane protein complexes that regulate the flow of ions across the membrane down their electrochemical gradients. They are involved in a wide variety of biological processes, such as cardiac, skeletal and smooth muscle contraction, T-cell activation, epithelial transport of nutrients and ions, as well as, pancreatic  $\beta$ -cell insulin release (41).

### **1.2.1 The potassium ion channels**

The most diverse class of cell membrane proteins are potassium channels which modulate the cell membrane potential and excitability. Potassium channels can be divided into four superfamilies, including calcium-activated potassium channels ( $K_{Ca}$ ), inwardly rectifying potassium channels ( $K_{ir}$ ), two-pore do-

main potassium channels ( $K_{2P}$ ) and voltage-gated potassium channels ( $K_v$ ) (according to the International Union of Basic and Clinical Pharmacology Criteria). Potassium channels are involved in vital cellular signalling processes in excitable and nonexcitable cells. These channels have been implicated in the regulation of neurotransmitter release, neuronal excitability, heart rate, insulin secretion, epithelial electrolyte transport, cell volume regulation, smooth muscle contraction and cell-cycle progression (42, 43).

### 1.2.2 hERG K<sup>+</sup> channels

The *human ether-a-go-go related gene* (official name *KCNH2*) encodes the pore-forming subunit of a delayed rectifier voltage gated K<sup>+</sup> (VGK) channel. The *human ether-a-go-go related gene* (hERG) was first cloned in 1994, by Warmke and Ganetzky, by screening a human hippocampal cDNA library with a mouse homologue of “ether-a-go-go” (EAG), a *Drosophila* K<sup>+</sup> channel gene (44).

hERG is predominantly expressed in the heart but it has also been found in brain regions, neuroendocrine glands and smooth muscle cells. In other species, transcripts are expressed strongly in the brain, slightly less in the heart, testis and lung, and with very low expression in skeletal muscle, adrenal gland and thymus (45).

hERG is the 11th member of the voltage gated K<sup>+</sup> channel family ( $K_v11.1$ ) (46). The functional channel is a tetramer, with each subunit containing six transmembrane domains (S1-S6) (Figure 3) (47). The S1-S4 domains of each subunit form the voltage sensor domain (VSD), while the S5-S6 domains together with P-loop form the pore domain (48). Additionally to the membrane-spinning region, hERG contains cytoplasmic NH<sub>2</sub>-terminal and COOH-terminal domains. The N-terminus contains a Per-Arnt-Sim (PAS) domain (about 135 amino acids) that defines the *ether-a-go-go* subfamily of voltage gated K<sup>+</sup> channels (49). The C-terminus contains a cyclic nucleotide binding domain (cNBD). The function of this domain is not well characterized. However, mutations in the cNBD domain are causing trafficking defects (50).

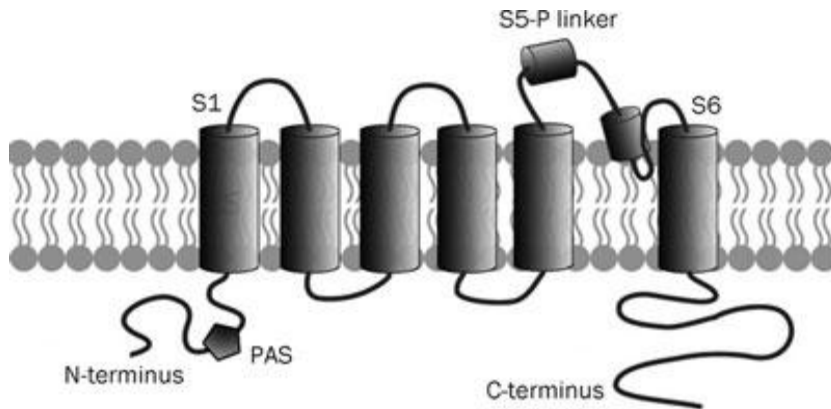


**Figure 3:** The basic structure of  $K_v11.1$  (48)

Although hERG has a similar structure to other potassium channels, it has unique gating kinetics, which are characterized by slow activation and deactivation but very rapid voltage-dependent inactivation, resulting into an outflow of a small current through it (51) (Figure 4). This is important in regards to the maintenance of the plateau phase of the action potential in atrial and ventricular myocytes (52). During depolarization, little outward current flows through the channels due to the slow activation and fast inactivation. As repolarisation begins, hERG channels recover from inactivation faster than they deactivate, generating an outward current. This outward current determines the termination of the plateau phase of the action potential.

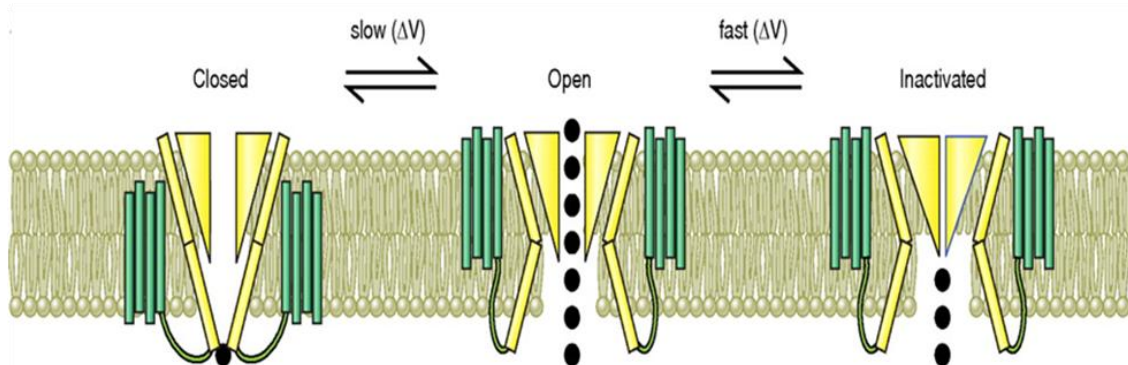


**Figure 4:** Gating of  $K_v11.1$  (modified from Vandenberg et al., 2012) (47)

### 1.2.3 hERG and the Long QT syndrome type 2 (LQT2)

$K_v 11.1$  channels play a crucial role in cardiac repolarisation, so the mutations that reduce the channel function have a negative effect on the cardiac electrical activity.

The inherited long QT syndrome (LQTS) is a heart condition, characterised by a prolonged QT interval in the electrocardiogram, syncope and sudden cardiac death due to ventricular tachyarrhythmia. It has been estimated that 1 in 2500 people worldwide is affected by congenital LQTS (53).

To date, nearly 300 different hERG mutations have been reported with a link to LQTS type 2 (48). These mutations are causing a reduction or defect of the protein synthesis, defective gating of the channel, impaired trafficking from the endoplasmic reticulum to the plasma membrane or defective ion permeation.

LQTS can also be acquired (aLQTS), which are associated with chronic heart failure or caused by a chemical blockade of the hERG channel. Many drugs have been removed from the market or terminated during clinical development due to suspected or confirmed cardiac side effects.

hERG defects can also cause stress-mediated arrhythmias, diabetes and myocardial ischemia induced arrhythmias (54). The hERG channel activators would accelerate the myocardial repolarisation and thus shorten the duration of the action potential. This can provide an alternative and more specific treatment for congenital and acquired LQTS. According to the latest reports, hERG activators may become a novel class of antiarrhythmic drugs (55).

#### **1.2.4 Other hERG channelopathies**

Several mutations in the *KCNH2* gene can result in the shortening of the QT interval (short QT syndrome) (56-58). People with the short QT syndrome have a higher risk of sudden cardiac death compared to patients with long QT intervals (59). Clinical trials of different hERG inhibitors have shown promising results in prolonging the QT interval to normal levels in patients with the short QT syndrome (60).

Parkington et al. have shown that changes in the hERG channel activity contribute to the electrophysiological mechanisms that produce contractions during labour. However, this system fails in obese women (61).

Recent investigations indicate a link between mutations in the *KCNH2* gene and epilepsy as well as developmental defects (62, 63).

### 1.2.5 hERG in cancer

The hERG channel is overexpressed in several human cancer cell lines (64). These include neuroblastoma, rhabdomyosarcoma, adenocarcinoma, monoblastic leukaemia, colon carcinoma (65-68). The hERG channel expression is associated with more aggressive tumours. The channel also modulates the invasiveness of cancer (69).

hERG channel blockers can reduce cell proliferation and induce apoptosis (70). However, only the specific targeted inhibitors should be used to reduce the side effects such as the prolonged QT syndrome, sudden death and cardiac arrhythmias (71).

## 1.3 Carrier proteins

Carrier proteins bind the specific solutes and transfer them across the membrane. This process resembles an enzyme-substrate reaction, however, the transported solute is not covalently modified by the carrier protein, but delivered unchanged to the other side of the membrane.

### 1.3.1 The sodium-glucose cotransporter SGLT1

SGLT1 is a member of the sodium/glucose cotransporter family SLC5 (72). There is only limited information available about the structure of SGLT1. SGLT1 consists of 14 transmembrane  $\alpha$ -helices, with an extracellular amino-terminus and an intracellular carboxyl-terminus. The COOH-terminal domain contains five terminal transmembrane helices, which are involved in sugar binding and translocation (Figure 5) (73).

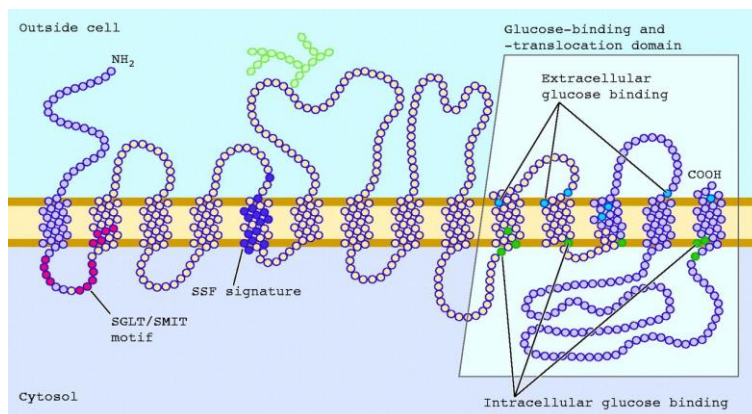


**Figure 5:** The secondary structure of SGLT1 (73)



SGLT1 is mainly expressed in the brush border membrane of the intestinal epithelium but also in the renal proximal tubule, in the heart, trachea, prostate and the salivary glands (73-75).

The sodium/glucose cotransporter SGLT1 simultaneously transports two Na<sup>+</sup> ions with one sugar molecule. D-glucose and D-galactose are preferred substrates for this carrier, whereas mannose is only slightly transported.

SGLT1 is responsible for the active transport of glucose across the brush border membrane of the small intestine and also plays an important role in water absorption either directly, as water cotransporter, or indirectly, as water channel (73). In the kidney, SGLT1 reabsorbs the glucose from the glomerular filtrate in the proximal tubule (76). SGLT1 may also behave as glucose receptor in the heart (73).

The mutations in the SGLT1 gene cause glucose-galactose malabsorption, a rare autosomal recessive disease, which manifests within the first weeks of life as a life-threatening diarrhea and dehydration (77).

Several studies indicate a functional role of SGLT1 in tumours (78-80). Cancer cells are well known to display an enhanced sugar uptake and consumption. This enhanced glucose uptake is partly is due to the induction of SGLT1 (80).

Another study shows a correlation between high SGLT1 and Bcl-2 expression in pancreatic primary tumours. The authors hypothesise that this can serve as prognostic markers in pancreatic cancer (78).

In another study, the link between glucose uptake by SGLT1, survival of cancer cells and EGFR (epidermal growth factor receptor) was revealed. Weihua et al. show that EGFR is able to maintain glucose uptake by cells through the SGLT1 stabilization, which promoted by the EGFR-SGLT1 interaction (81). Therefore, the survival of cancer cells is promoted by maintenance of intracellular glucose level.

### **1.3.2 The sodium-coupled phosphate cotransporters NaPi-IIa and NaPi-IIb**

Phosphorus is one of the most abundant minerals in the body. It is required for cell metabolism (signaling and energy production), skeletal development, protein synthesis and bone mineralization (82).

The extracellular and intracellular phosphate levels are maintained within a narrow range for an optimal cellular function. This is achieved by intestinal phosphate uptake, renal reabsorption and excretion as well as the exchange of phosphate between extracellular and bone storage pools (83). The kidney and the small intestine are the main organs to maintain phosphorus homeostasis. The Na<sup>+</sup>-coupled phosphate cotransporter NaPi-IIa belongs to the SLC34 family (SLC34A1) and is located at the apical membrane of renal proximal tubular cells (84). The NaPi-IIa protein is also detected in rat brain, osteoblast-like cells and osteoclasts (85-87). The amount of NaPi-IIa gradually decreases along the proximal tubule, with the highest level in the S1 segment.

The Na<sup>+</sup>-coupled phosphate cotransporter NaPi-IIa mediates the electrogenic transport of inorganic phosphate coupled to three sodium ions. Moreover, NaPi-IIa prefers divalent inorganic phosphate (HPO<sub>4</sub><sup>2-</sup>) (84).

The basic transmembrane transport cycle for NaPi-IIa can be described in several steps. Firstly, two Na<sup>+</sup> ions bind sequentially (the intrinsic charge senses the transmembrane field and this allows binding of the first sodium ion), then the binding of divalent P<sub>i</sub> follows and finally the binding of a third Na<sup>+</sup> ion takes place. The reorientation of the fully loaded carrier occurs and the substrate releases to the cytosol. After all substrates have been released to the cytosol, the intrinsic charge senses the transmembrane field, leading to a voltage-dependent reorientation of the empty carrier (82).

The possible structural information for the Na<sup>+</sup>-coupled phosphate cotransporter NaPi-IIa is based on indirect biochemical and biophysical studies on wild-type and engineered mutants (84, 88). The model consists of 12 transmembrane-spanning domains. NH<sub>2</sub>- and COOH-termini are located intracellularly and two N-glycosylation sites are located in a large extracellular loop (Figure 6) (84). The COOH terminus is important for the hormonal regulation, targeting and protein-protein interactions (82).

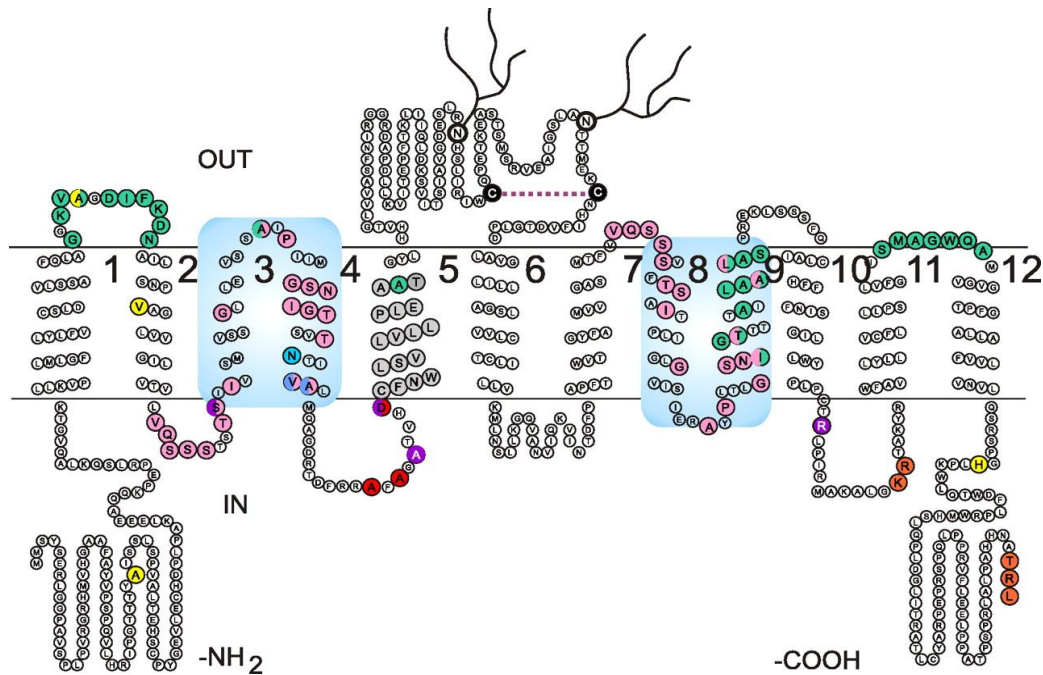


**Figure 6:** Topological model of NaPi-IIa (84)

NaPi-IIa is assumed to be a functional monomer. However, there is evidence that SLC34 proteins may exist as dimers or even possibly tetramers (89, 90). The NaPi-IIa transporter is regulated by different factors, including dietary phosphate and acid–base status, parathyroid hormone, 1,25-dihydroxyvitamin D<sub>3</sub>, FGF23, growth hormone, insulin-like growth factor IGF1 and insulin (91, 92). The NaPi-IIa knockout mice display a phenotype consisting of hyperphosphaturia that indicates the critical role of this transporter in phosphate homeostasis (93). The dysregulation of NaPi-IIa causes phosphate deficiency disorders, such as X-linked hypophosphatemia and autosomal-dominant hypophosphatemic rickets (92).

Several mutations in the NaPi-IIa gene were described. However, the role of these mutations on renal phosphate balance and kidney function remains uncertain. Some data suggest that the mutations alone are not responsible for the disease in the patients (92).

Another member of the solute carrier family SLC34 is NaPi-IIb (SLC34A2), localized in the brush-border membrane of enterocytes and in colon, lung, testes, liver, mammary gland, uterus and thyroid gland (94). NaPi-IIb is responsible for the transcellular phosphate absorption in the small intestine (95). Xu Y. et al.

reported the expression of NaPi-IIb in the murine epididymis and its potential role in the male fertility regulation (96). In the rat liver, NaPi-IIb is involved in the reabsorption of phosphate from the bile (97). The NaPi-IIb cotransporter is expressed apically in lactating mammary gland, which suggests its role in the milk secretion (98). In salivary glands, NaPi-IIb is involved in secreting  $P_i$  into saliva (99).

The  $Na^+$ -coupled phosphate cotransporter NaPi-IIb shares some similarities to NaPi-IIa. Both of them are electrogenic and transport phosphate with stoichiometry of 3:1 ( $Na^+$ :  $HPO_4^{2-}$ ) (83).

The bioinformatics analyses suggested that NaPi-IIb contains at least eight transmembrane domains with both N- and C-terminal regions located in the cytoplasm (100). The mass spectrometry determined the existence of monomeric and dimeric forms of the protein (100). It has been shown that NaPi-IIb is regulated by a number of factors, including dietary phosphate load, 1,25-dihydroxyvitamin  $D_3$ , growth factors etc. (96).

The different mutations in the SLC34A2 gene have been described, which lead to the accumulation of phosphate in the organs where the transporter is expressed. The most of these mutations are associated with the pulmonary alveolar microlithiasis and/or testicular microlithiasis (101, 102). The altered expression of NaPi-IIb was detected in several cancers such as ovarian, papillary thyroid and breast cancer (103-105).

## 1.4 Aim of the study

From the studies published so far, it became evident that B-RAF plays an essential role in the activation of the RAS/RAF/MEK/ERK signalling pathway, which controls cellular proliferation, differentiation and survival (106). Dysregulated B-RAF signaling has been the subject of intense investigation in oncology after Davies et al. reported that this kinase is mutated in approximately 7% of human tumours (32). Moreover, B-RAF kinase represents an excellent target for anticancer drug development. However, just limited amount of data exist on the role of B-RAF in the regulation of the ion channels and transporters. Thus, this thesis aims to identify novel ion channels and carriers that may be regulated by B-RAF.

In view of the importance of hERG channels in the tumour cell proliferation and apoptosis and considering that B-RAF is up-regulated in tumour cells, this work explores whether B-RAF may participate directly in the regulation of these channels, by using the *Xenopus* oocytes expression system. Additionally, this thesis determines the effect of the B-RAF inhibitor PLX-4720 on the hERG-mediated current and the hERG protein abundance in *Xenopus* oocytes and in rhabdomyosarcoma RD cells.

Furthermore, several studies revealed a functional role of SGLT1 in malignant tumours. This work investigates the role of B-RAF in the regulation of this carrier.

Moreover, it was previously shown that B-RAF contributes to signalling of the insulin-like growth factor IGF1. The effects of IGF1 include a stimulation of the proximal renal tubular phosphate transport, accomplished in a large part by NaPi-IIa. NaPi-IIb accomplishes the transport of phosphate in the intestine and its altered expression was detected in several cancers. Therefore, this work explores whether B-RAF influences the protein abundance and/or activity of the type II sodium-coupled phosphate cotransporters NaPi-IIa and NaPi-IIb, expressed in *Xenopus* oocytes. This thesis also determines the effect of the B-RAF inhibitor PLX-4720 on the NaPi-IIa cell surface protein abundance in HEK293 cells.

## 2 Materials and methods

In order to express hERG channels, SGLT1, NaPi-IIa and NaPi-IIb transporters in *Xenopus* oocytes, DNA constructs were linearized with the appropriate restriction enzymes. Then linearized DNA was used as a template for *in vitro* transcription using the suitable RNA polymerases. The heterologous cRNA was injected into prepared *Xenopus* oocytes and after full expression of the proteins, the two-electrode voltage clamp technique was used for functional studies. To determine the protein abundance of hERG, SGLT1, NaPi-IIa and NaPi-IIb in *Xenopus* oocytes, immunocytochemistry with confocal microscopy was used as well as chemiluminescence. For the experiments in mammalian cells, rhabdomyosarcoma RD cells and HEK293 cells were routinely cultured in the appropriate medium. To quantify the effect of the B-RAF inhibitor on the cell surface expression and the hERG mediated current, the biotinylation of the cell surface proteins and flow cytometry as well as whole-cell patch clamp techniques were employed. Additionally the effect of the B-RAF inhibitor on the NaPi-IIa cell surface expression was determined by biotinylation of the cell surface proteins and subsequently western blot technique.

### 2.1 Constructs and cRNA synthesis

For protein expression in *Xenopus laevis* oocytes the following constructs were used: human wild-type B-RAF (Imagenes, Berlin, Germany) (107), hERG (44), hERG-HA (108) containing an extracellular hemagglutinin epitope, wild-type human SGLT1 (109) (SLC5A1), wild-type human NaPi-IIa (110), wild-type mouse NaPi-IIb (94) inserted into the appropriate vector.

The plasmids were transformed into DH5 $\alpha$  *E. coli* competent cells (Invitrogen, Life Technologies, Carlsbad, CA, USA) according to the manufacturer's instruction. The transformation was plated onto LB agar (Carl Roth, Karlsruhe, Germany) plate containing 100  $\mu$ g/ml ampicillin (Carl Roth, Karlsruhe, Germany) and incubated overnight at 37°C.

A single colony was inoculated in 50 ml of LB medium (Carl Roth, Karlsruhe, Germany) supplemented with 100  $\mu$ g/ml ampicillin (Carl Roth, Karlsruhe, Germany). Flask was incubated for 12-16 hours at 37°C in the incubator with vigor-

ous shaking (220-250 rpm). The cells were centrifuged for 20 minutes (4000 x g) at 4°C. The plasmids were purified with NucleoBond Xtra Midi kit (Macherey – Nagel GmbH, Dueren, Germany) according to the manufacturer’s instruction. The DNA concentration was estimated by UV absorbance at 260 nm. The plasmid purity also was checked by UV spectroscopy. A ratio  $A_{260}/A_{280}$  between 1.8-1.9 and  $A_{260}/A_{230}$  around 2.0 indicates the pure plasmid. The plasmid should be linearized prior its use as a template for *in vitro* transcription with the restriction enzyme which cuts behind the 3’-end of the cloned cDNA fragment. The sample reaction was made in a final volume of 50 µl and containing 10 µg of plasmid DNA, 5 µl of 10x Reaction Buffer (New England Biolabs GmbH, Frankfurt am Main, Germany), 5 µl of 10x BSA (if restriction enzyme require) (New England Biolabs GmbH, Frankfurt am Main, Germany), 2.5 µl of restriction enzyme (New England Biolabs GmbH, Frankfurt am Main, Germany). The reaction was mixed and incubated for 1-2 hours at the temperature optimal for enzyme on the thermostat. Table 1 shows the specific endonucleases used for linearization of the plasmids.

**Table 1:** Restriction enzymes used for linearization of the constructs

Plasmid	Vector	Restriction enzyme
human wild type B-RAF	pCMV-SPORT6	XhoI
hERG	pSP64	EcoRI
hERG-HA	pSP64	EcoRI
human SGLT1	pBluescript	EcoRI
human NaPi-IIa	KSM	XbaI
mouse NaPi-IIb	pSPORT1	Sall

The linearized DNA was purified with NucleoSpin Extract II kit (Macherey – Nagel GmbH, Dueren, Germany) according to the instruction manual. The integrity and size of the linearized DNA were confirmed by agarose gel electrophoresis. The purity was checked by UV spectroscopy. A ratio  $A_{260}/A_{280}$  between 1.8-1.9 and  $A_{260}/A_{230}$  around 2.0 indicates the pure linearized DNA.

For cRNA synthesis, it is essential to avoid RNase contamination by using gloves, sterile glassware and DEPC water.

*In vitro* synthesis of RNA was made by using T3 or SP6 RNA polymerases (New England Biolabs GmbH, Frankfurt am Main, Germany) (see Table 2). The sample reaction contained: 1 µg linearized DNA, 2.5 µl 10x reaction buffer (New England Biolabs GmbH, Frankfurt am Main, Germany), 1 µl rNTPs (Roche, Mannheim, Germany), 2.5 µl Cap analog m<sup>7</sup>G(5')ppp(5')G (New England Biolabs GmbH, Frankfurt am Main, Germany), 1 µl RNase inhibitor (New England Biolabs GmbH, Frankfurt am Main, Germany) and 1 µl RNA polymerase in the final reaction volume of 25 µl. The reaction was mixed and incubated for 2-3 hours at 37°C on the thermostat.

To remove the plasmid DNA template after RNA synthesis 1 µl of DNaseI (New England Biolabs GmbH, Frankfurt am Main, Germany) was added for 15 minutes at 37°C.

RNA was purified using MEGAclear purification kit (Ambion, Life Technologies, Carlsbad, CA, USA) according to the manufacturer's instruction. The concentration of RNA was determined by reading the absorbance in a spectrophotometer at 260 nm. The integrity of the transcripts was confirmed by agarose gel electrophoresis (see 2.2). RNA was stored at -80°C until the injection.

**Table 2:** RNA polymerases used to prepare cRNA

<b>Construct</b>	<b>RNA polymerase</b>
human wild type B-RAF	SP6
hERG	SP6
hERG-HA	SP6
human SGLT1	T3
human NaPi-IIa	T3
mouse NaPi-IIb	SP6

## 2.2 Agarose gel electrophoresis

To prepare 100 ml of 1% agarose gel we used: 100 ml TAE buffer, 1 g agarose powder (Lonza, Rockland, ME, USA). The solution was microwaved for 1-3 minutes until it was completely dissolved. The solution was cooled down for 5 minutes and the SYBR Safe DNA gel stain (diluted 1:10000; Invitrogen, Eugene, OR, USA) was added. The agarose was poured into the gel tray with the comb in place. It was solidified at room temperature. The gel box was filled



with 1x TAE buffer (50x stock solution: 242 g Tris base, 57.1 ml glacial acetic acid, 100 ml 0.5 M EDTA, filled up to 1 litre with distilled water). The samples were mixed with 6x loading buffer (Carl Roth GmbH, Karlsruhe, Germany) and loaded on the agarose gel along with 1 kb DNA marker (Carl Roth GmbH, Karlsruhe, Germany). The gel was run at 100 mV until the dye line was 75-85% of the way down the gel. DNA fragments were visualized by analysing the gel on an UV transilluminator (Bio-Rad, Munich, Germany). Using the DNA ladder the size of separated DNA fragments was interpreted.

### **2.3 Heterologous expression of the ion channels and transporters in *Xenopus laevis* oocytes**

*Xenopus laevis* oocytes are widely used for the expression of mammalian transporters and channels due to their ability to efficiently translate exogenous mRNA into proteins. On the other hand, it is an inexpensive, easily manipulated method and large amounts of material can be readily obtained for a variety of experimental procedures. *Xenopus laevis* oocytes express only a small number of endogenous membrane transport systems, which give a low background to the heterologously expressed proteins.

### **2.4 *Xenopus laevis* oocytes preparation and maintenance**

All animal experiments were conducted according to the recommendations of the Guide for Care and Use of Laboratory Animals of the National Institutes of Health as well as the German law for the welfare of animals. The experiments were reviewed and approved by the respective government authority of the state Baden-Württemberg (Regierungspräsidium) prior to the start of the study (Anzeige für Organentnahme nach §6 Tierschutzgesetz).

The adult female *Xenopus laevis* frogs (NASCO, Fort Atkinson, USA) were anaesthetized by submersion in 0.1% Tricaine solution (ethyl 3-aminobenzoate methanesulfonate salt, Sigma, Steinheim, Germany) for 15-20 minutes and placed on ice for surgery. After confirmation of anaesthesia and disinfection of the skin, a small abdominal incision was made and the oocytes were removed carefully without injuring any blood capillaries, followed by the closure of the

skin by sutures. All efforts were made to minimize animal suffering. The frogs were kept wet but not under water until reflexes were fully recovered to prevent drowning. The ovarian lobes were manually separated and the oocytes were enzymatically defolliculated by treatment with a  $\text{Ca}^{2+}$ -free OR2 solution (in mmol/l), 82.5 NaCl, 2 KCl, 1  $\text{MgCl}_2$  and 5 HEPES, titrated to pH 7.4 with NaOH, 200 mOsm/l, containing 1 mg/ml collagenase Type II (Worthington Biochemical Corporation, Lakewood, NJ, USA) for 1 hour shaken at room temperature. Then the collagenase solution was changed and the oocytes were incubated for another hour shaking at room temperature. To remove all debris and collagenase, the oocytes were washed 4 to 6 times in fresh  $\text{Ca}^{2+}$ -free OR2 solution. In order to stop defolliculation, the oocytes were washed 10 times with ND96 solution (in mmol/l) 96 NaCl, 2 KCl, 1.8  $\text{CaCl}_2$ , 1  $\text{MgCl}_2$  and 5 mM HEPES, titrated to pH 7.4 with NaOH. The oocytes on the stages V-VI were selected (sharp equatorial boundary can be observed between pigmented animal pole and the vegetal pole) and stored at 18°C in ND96 solution, supplemented with 0.11 mM tetracycline (Sigma, Steinheim, Germany), 4  $\mu\text{M}$  ciprofloxacin (Fresenius, Bad Homburg, Germany), 0.2 mM refobacin (MerckSerono, Darmstadt, Germany), 0.5 mM theophylline (Takeda, Singen, Germany) and 5 mM sodium pyruvate (Sigma, Steinheim, Germany).

## **2.5 cRNA injection**

For the injection of cRNA a Nanoliter-Injector 2000 (World Precision Instruments, Berlin, Germany) with glass capillaries (WPI, Sarasota, FL, USA), mounted in a micromanipulator, was used. The injection was performed on the day when the oocytes were withdrawn or the next day. To prevent a contamination with RNAases, only pipettes dedicated for RNA work as well as certified nuclease-free labware, sterile filter tips and DEPC treated water for dilution of cRNA were used. The glass capillaries were pulled using an automatic micro-electrode puller DMZ Universal Puller (Zeitz Instruments, Augsburg, Germany). The tip was mechanically broken off with forceps (diameter 10-20  $\mu\text{m}$ ). The needle was backfilled with mineral oil (avoiding air bubbles) and assembled into the nanoinjector. Approximately 3  $\mu\text{l}$  of cRNA solution were loaded into the in-

jection capillary. The oocytes were transferred into a grid network and injected with a required volume of cRNA (see Table 3). After injection, the oocytes were kept in Petri dishes containing ND96 solution supplemented with antibiotics at 17°C. The storage solution was exchanged on a daily basis to increase the oocytes survival.

**Table 3:** Amount of cRNA injected into *Xenopus laevis* oocytes

<b>Construct</b>	<b>cRNA (ng/oocyte)</b>	<b>Expression time (days)</b>
hERG	10	3
hERG-HA	10	3
human NaPi-IIa	10	3
mouse NaPi-IIb	15	3-4
human SGLT1	10	3
human wild type B-RAF	10	3

After full expression of the proteins, functional studies were performed.

## **2.6 Electrophysiological measurements**

Ion channels and transporters expressed in *Xenopus* oocytes were studied by using the two-electrode voltage clamp (TEVC) technique. Two microelectrodes were inserted through the membrane of the oocyte. The first, voltage sensing, electrode monitored the voltage of the cell membrane. To keep the membrane potential at a desired level, a current was injected by the second electrode. This membrane current was recorded and reflected the ion channel activities. Figure 7 illustrates the principle of TEVC.

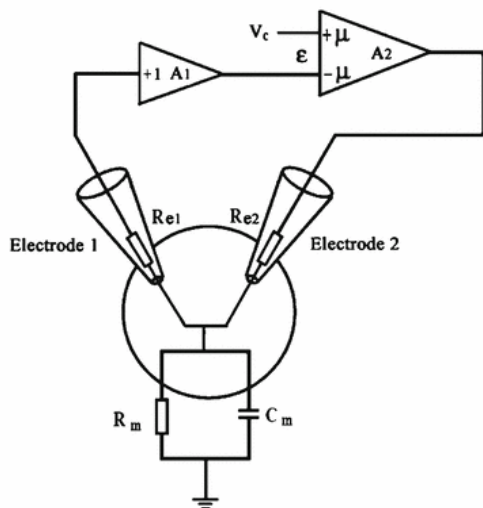


**Figure 7:** Two-electrode voltage clamp on *Xenopus* oocyte (111)

For all recordings with TEVC, the pipettes were filled with 3 M KCl and had the resistances of 0.3-3.0 M $\Omega$ . The data were filtered at 1 Hz (hERG) or 10 Hz (NaPi-IIa, NaPi-IIb, SGLT1) and recorded with a Digidata A/D-D/A converter and Clampex 9.2 software for data acquisition and analysis (Axon Instruments, Union City, CA, USA). The analysis of dual-electrode voltage clamp data was performed with Clampfit 9.2 (Axon instruments, Union City, CA, USA). To measure hERG channels, the holding potential was kept at -80 mV and the outward tail currents were elicited by voltage pulses to a potential of -60 mV for 500 ms after the preconditioning steps to potentials between -80 and +70 mV for 500 ms. The leak currents estimated from the tail current measured after the preconditioning prepulse to -80 mV were subtracted. For normalization, the individual tail currents at +70 mV were divided by the mean tail current at +70 mV of *Xenopus* oocytes expressing hERG alone.

The TEVC recordings of NaPi-IIa and NaPi-IIb transporters were performed at a holding potential of -60 mV. The control superfusate (ND96) contained (in mmol/l) 96 NaCl, 2 KCl, 1.8 CaCl<sub>2</sub>, 1 MgCl<sub>2</sub> and 5 HEPES, titrated to pH 7.4 with NaOH. Phosphate was added to the solutions at a concentration of 1 mmol/l unless otherwise stated. The flow rate of the superfusion was approximately 20 ml/min, and a complete exchange of the bath solution was reached within about 10 seconds.

SGLT1 TEVC recordings were performed at a holding potential of -70 mV. The control superfusate (ND96) contained (in mmol/l) 96 NaCl, 2 KCl, 1.8 CaCl<sub>2</sub>, 1 MgCl<sub>2</sub> and 5 HEPES, titrated to pH 7.4 with NaOH. Glucose was added to the solutions at a concentration of 10 mmol/l unless otherwise stated. The flow rate of the superfusion was approximately 20 ml/min, and a complete exchange of the bath solution was reached within about 10 seconds.

## 2.7 Whole-cell patch clamp

The patch clamp experiments were performed at room temperature in voltage clamp, fast-whole-cell mode according to Hamill et al. (112). The cells were continuously superfused through a flow system inserted into the dish. The currents were recorded by EPC-9 amplifier (Heka, Lambrecht, Germany) using Pulse software (Heka) and ITC-16 Interface (Instrutech, Port Washington, NY, USA). The currents were elicited by voltage pulses to a potential of -120 mV for 500 ms after preconditioning steps at potentials between -80 and +60 mV for 2 seconds. Leak currents estimated from the tail current measured after the preconditioning prepulse to -80 mV were subtracted. The currents were recorded with an acquisition frequency of 10 kHz and 3 kHz low-pass filtered. The liquid junction potential  $\Delta E$ , between pipette and bath solutions, was estimated according to Barry and Lynch (113) and corrected. The cells were superfused with a bath solution containing (in mmol/l): 92 NaCl, 40 KCl, 2 CaCl<sub>2</sub>, 2 MgCl<sub>2</sub>, 5 glucose and 10 HEPES/NaOH, pH 7.4. The pipettes were filled with an internal solution at a  $[Ca^{2+}]_i$  of  $10^{-7}$  M (pCa 7) containing (in mmol/l) 120 K-gluconate, 10 NaCl, 2 MgCl<sub>2</sub>, 4 CaCl<sub>2</sub>, 10 EGTA/KOH, 10 HEPES/KOH, 3 Mg-ATP, pH 7.3.

## 2.8 Flow cytometry

One of the widely used applications of the flow cytometry is analysis of cell surface proteins. This technique allows multi-parameter analysis of a single cell and based on measuring the fluorescence intensity produced by fluorescent-labelled antibodies bind to the proteins of the interest. Figure 8 illustrates the principle of the experiment.

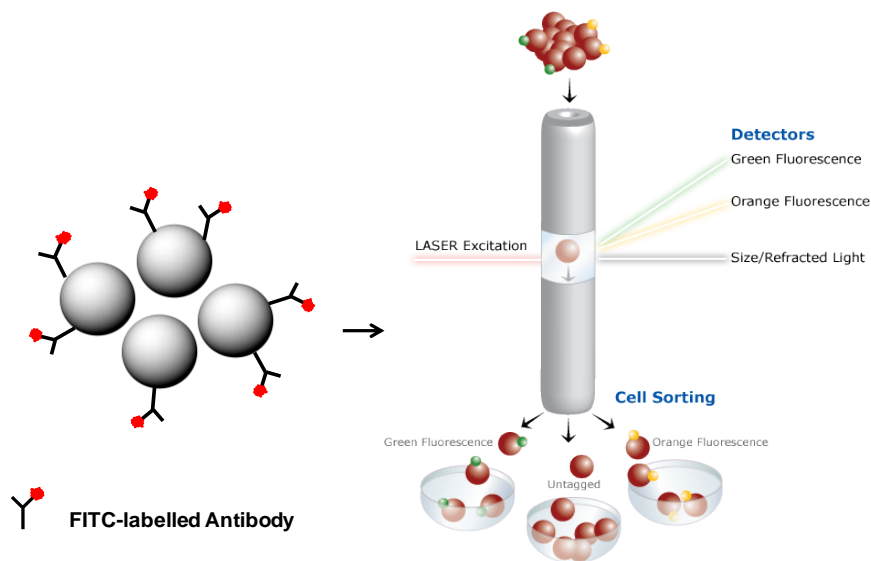


**Figure 8:** Detection of cell surface protein expression by flow cytometry (GenWay Biotech Inc., San Diego, CA, USA)

The rhabdomyosarcoma RD cells were washed once with PBS, detached from the plates by incubation for 10 minutes with Versene solution (Life Technologies, Gibco, USA) at 37°C, 5% CO<sub>2</sub>. The cells were centrifuged for 5 minutes at 1200 rpm.  $1 \times 10^6$  cells in 25  $\mu$ l of PBS were stained 20 minutes with 1  $\mu$ l anti-Kv11.1 (hERG, extracellular)-FITC antibody (Alamone Labs, Jerusalem, Israel). The forward scatter of the cells was determined and hERG-FITC fluorescence intensity was measured in FL-1 with an excitation wavelength of 488 nm and an emission wavelength of 530 nm on a flow cytometer (FACSCalibur, BD Biosciences, USA).

## 2.9 Biotinylation of cell surface proteins

The biotinylation technique is used to label, isolate and analyze cell surface proteins. The biotinylation reagent forms a stable complex with membrane proteins. Treated cells then harvested, lysed and labelled proteins are isolated using immobilized avidin or streptavidin (avidin-biotin binding is the strongest known non-covalent interaction between a protein and ligand).

To analyze hERG cell membrane abundance, rhabdomyosarcoma RD cells and to analyze NaPi-IIa cell membrane abundance HEK293, cells were washed twice with ice-cold PBS. Then cells were labelled with 250  $\mu$ g/ml Sulfo-NHS-LC-

biotin (Pierce, Rockford, IL, USA) in PBS for 30 minutes at 4°C. The Sulfo-NHS-LC-biotin bound to the membrane proteins was quenched with 50 mM Tris-HCl buffer pH 7.4. After washing, the cells were lysed with ice-cold RIPA buffer (Cell Signaling, Danvers, MA, USA) supplemented with the complete protease and phosphatase inhibitor cocktail (Thermo Fisher Scientific, Rockford, IL, USA). After centrifugation at 10000 rpm for 5 minutes, protein concentration was determined by Bradford assay (Bio-Rad Laboratories, Hercules, CA, USA). 200 µg of proteins were supplemented with 50 µl washed immobilized NeutrAvidin Agarose beads (Pierce, Rockford, IL, USA) and incubated at 4°C overnight on a rotator. The beads were then pelleted by 1 minute centrifugation at 13000 rpm and washed 3 times in PBS containing 1% NP-40 / 0.1% SDS and twice in 0.1% NP-40 / 0.5 M NaCl. The proteins were solubilised in Roti-Load1 buffer (Carl Roth GmbH, Karlsruhe, Germany) at 95°C for 10 minutes.

## 2.10 Western blotting

### 2.10.1 The SDS polyacrylamide gel electrophoresis (SDS-PAGE)

SDS-PAGE is used to separate the proteins according to their size.

The 8% (for hERG) and 10% (for NaPi-IIa) separating gels were prepared according to Table 4.

**Table 4:** Composition of separating acrylamide gels

Acrylamide percentage	8%	10%
H <sub>2</sub> O	4.6 ml	3.8 ml
30% Acrylamide mix (29:1 acrylamide:bis-acrylamide)	2.6 ml	3.4 ml
1.5 M Tris (pH = 8.8)	2.6 ml	2.6 ml
10%(w/v) SDS	0.1 ml	0.1 ml
10% (w/v) ammonium persulfate	0.1 ml	0.1 ml
TEMED	0.01 ml	0.01 ml
Total volume	10 ml	10 ml

The separating gel was gently overlaid with 2-Propanol to shield the buffer from air which will inhibit the polymerization. After polymerization, the gel surface was rinsed with distilled water. The top of the separating gel was dried with filter

paper. After it was laid with 5% stacking gel (for 10 ml: 6.8 ml ddH<sub>2</sub>O, 1.7 ml 30% acrylamide mix, 1.3 ml 1 M Tris (pH = 6.8), 0.1 ml 10% SDS, 0.1 ml 10% APS, 0.01 ml TEMED) and a comb was placed. The gel was allowed to polymerize. The glass plates were assembled in the Mini-PROTEAN Tetra cell electrophoresis module according to the manufacturer instructions (Bio-Rad, Munich, Germany). The module was filled with 1x running buffer (Carl Roth GmbH, Karlsruhe, Germany) and the samples were loaded along with a prestained molecular weight marker (PEQLAB, Erlangen, Germany). Mini-PROTEAN Tetra Tank (Bio-Rad, Munich, Germany) was assembled and the gels were run at 80 / 120 mV for 2-2.5 hours until the protein marker almost reached the foot line of the glass plate.

### **2.10.2 Protein transfer to a membrane and protein detection**

The transfer buffer was prepared (10x buffer pH 8.3: 24 g Tris base, 113 g glycine, fill with distilled H<sub>2</sub>O up to 1 l). The PVDF membrane was used for the proteins transfer. The mini Trans-Blot Cell (Bio-Rad, Munich, Germany) was assembled according to the manufacture guideline. The blot was run for 1 hour at 100 mV. The membrane was blocked with 5% non-fat dry milk (Carl Roth GmbH, Karlsruhe, Germany) in TBS 0.1% Tween 20 (TBST) for 1 hour at room temperature. The membrane was incubated overnight at 4°C with rabbit anti-Kv11.1 (hERG, extracellular) antibody (diluted 1:200, Alamone Labs, Jerusalem, Israel) or rabbit anti-human SLC34A1 (NaPi-IIa) polyclonal antibody (diluted 1:500, Life Span Biosciences, WA, USA). After washing in TBST (10x TBS, pH = 7.4: 87.7 g NaCl, 30.3 g Tris base, fill with ddH<sub>2</sub>O up to 1 l), blots were incubated with anti-rabbit HRP-conjugated antibody (diluted 1:1000, Cell Signaling, Danvers, MA, USA) for 1 hour at room temperature. The antibody binding was detected with the ECL detection reagent (Amersham, Freiburg, Germany) and the bands were quantified with the Quantity One Software (Bio-Rad, Munich, Germany).



## 2.11 Detection of cell surface protein expression by chemiluminescence

The chemiluminescence occurs when a chemical substrate is catalyzed by an enzyme, such as horseradish peroxidase (HRP), and produces light as a by-product, which can be quantified in a luminometer. This technology is adapted for the detection of the membrane-bounded proteins while the chemiluminescence uses enzyme-conjugated antibodies to activate the light signal. Figure 9 illustrates general principal of the method.

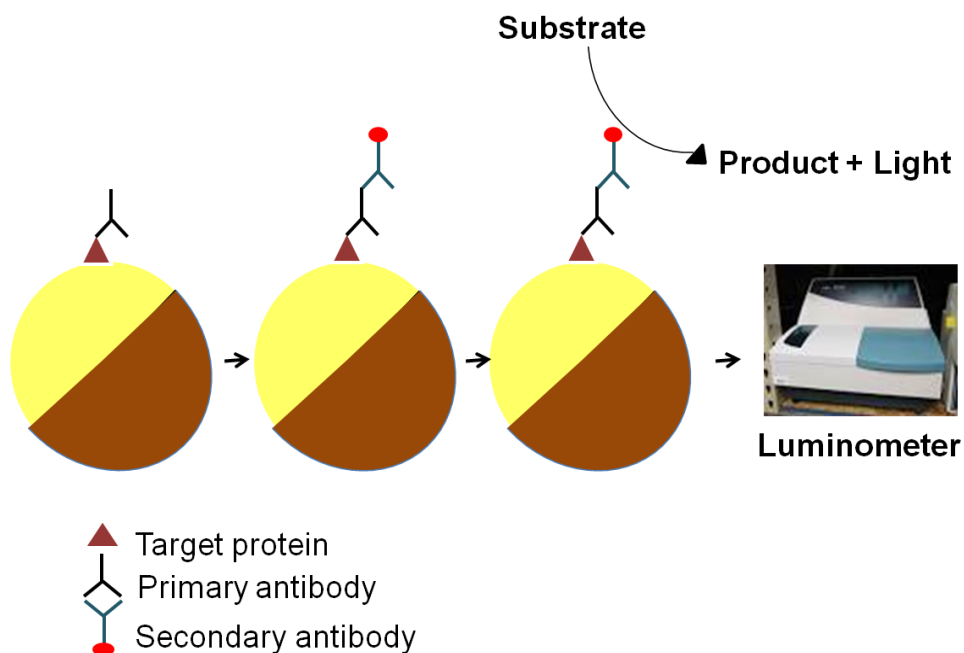


**Figure 9:** Detection of cell surface protein expression by chemiluminescence in *Xenopus* oocytes

The oocytes expressing hERG with an external HA-tag were blocked for 20 minutes in ND96 (see chapter 3.9) solution with 1% BSA at 4°C. The oocytes were incubated with 0.5 µg/ml primary rat monoclonal anti-HA antibody diluted in 1% BSA / ND96 (clone 3 F10, Roche, Mannheim, Germany) for 1 hour at 4°C. After incubation with primary antibody, the oocytes were washed 3 times for 5 minutes at 4°C with 1% BSA / ND96. Next, the secondary HRP-conjugated goat anti-rat antibody (diluted 1:1000, Cell Signaling Technology, MA, USA) was added to the oocytes and incubated for 1 hour on ice. Then they were

washed 5 times for 5 minutes each in 1% BSA / ND96 and then 5 times in ND96 without BSA on ice.

To detect SGLT1 cell surface expression, the oocytes were incubated with rabbit polyclonal anti-SGLT1 antibody (diluted 1:1000, Millipore, MA, USA) and subsequently with secondary, HRP-conjugated anti-rabbit antibody (diluted 1:1000, Cell Signaling Technology, MA, USA). To determine the NaPi-IIa cell surface expression, the oocytes were incubated with primary rabbit anti-human SLC34A1 (NaPi-IIa) polyclonal antibody (diluted 1:500, Life Span Biosciences, WA, USA) and after with secondary, HRP-conjugated goat anti-rabbit IgG antibody (diluted 1:1000, Cell Signaling Technology, MA, USA). Blocking time, incubation with primary and secondary antibodies as well as washing step was the same in all three experiments.

Individual oocytes were placed in 96 well plates with 100  $\mu$ l of ND96 and 20  $\mu$ l of the SuperSignal ELISA Femto Maximum Sensitivity Substrate (Pierce, Rockford, IL, USA). The chemiluminescence of the single oocyte was quantified in Wallac Victor2 plate reader (Perkin Elmer, Juegesheim, Germany) by integrating the signal over a period of 1 second. The results display normalized relative light units. The integrity of the measured oocytes was assessed by visual control after the measurement to avoid unspecific light signals from the cytosol.

## **2.12 Immunocytochemistry and confocal microscopy**

To visualize specific protein, primary antibody used against the target molecule, followed by binding of fluorochrome-conjugated secondary antibody. The complex can be visualized on laser excitation of the fluorochrome at the certain wavelength. The confocal microscope detects the emission of energy at the given wavelength. The scheme of the experiment illustrated in Figure 10.

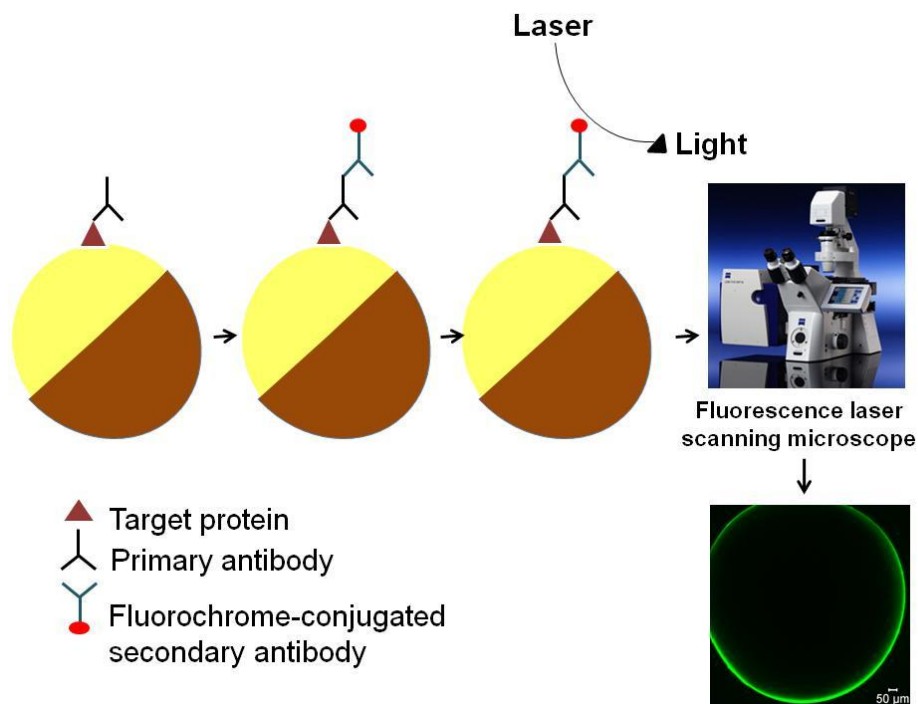


**Figure 10:** Detection of cell surface protein expression by immunocytochemistry and confocal microscopy in *Xenopus* oocytes

To visualize the hERG-HA and NaPi-IIa protein abundance, the oocytes were fixated in 4% paraformaldehyde / PBS for at least 4 hours. Then the oocytes were cryoprotected in 30% sucrose / PBS overnight at 4°C, frozen in mounting medium TissueTek (Sakura, Zoeterwoude, Netherlands) and placed on a cryostat. The sections were collected at a thickness of 8 μm on the coated slides and stored at -80°C. For immunostaining, the slides were dried at room temperature, fixed in acetone / methanol (1:1) for 15 minutes, washed in PBS 3 times and blocked for 1 hour in 5% bovine serum albumin / PBS. The primary antibody used was rat monoclonal anti-HA antibody (1 μg/ml, clone 3 F10, Roche, Mannheim, Germany) or rabbit anti-human SLC34A1 (NaPi-IIa) polyclonal antibody (diluted 1:100, Life Span Biosciences, WA, USA). The slides were incubated in a moist chamber overnight at 4°C. The binding of primary antibody was visualised with anti-rat Alexa488-conjugated antibody (diluted 1:200, Invitrogen, UK) or FITC-conjugated goat anti-rabbit IgG (diluted 1:1000, Invitrogen, Molecular Probes, Eugene, OR, USA) for 1 hour at room temperature. The slides were mounted with ProLong Gold antifade reagent (Invitrogen,

UK). Images were taken on a fluorescence laser scanning microscope LSM 510 (Carl Zeiss MicroImaging, Goettingen, Germany) with A-Plan 40x/1.2W DICIII. The brightness and contrast settings were kept constant during imaging of all oocytes in each injection series. Due to autofluorescence of the oocyte yolk, unspecific immunofluorescence was observed inside the *Xenopus* oocytes.

For detection of SGLT1 membrane abundance, the oocytes were fixed in 4% paraformaldehyde at room temperature for 2 hours. After washing with phosphate buffered saline (PBS), the oocytes were permeabilized and blocked at room temperature for 1 hour in TBS (Tris Buffered Saline), containing 0.1% TritonX-100 and 10% normal goat serum. Then, the oocytes were incubated overnight at 4°C with primary rabbit polyclonal anti-SGLT1 antibody (diluted 1:1000, Millipore, MA, USA) followed by 30 minutes incubation at 37°C with FITC-Goat anti-rabbit IgG (diluted 1:1000, Invitrogen, Molecular Probes, Eugene, OR, USA). Next, the oocytes were analyzed by a fluorescence laser scanning microscope LSM 510 (Carl Zeiss MicroImaging, Goettingen, Germany) with A-Plan10x / 0.25. The brightness and contrast settings were kept constant during imaging of all oocytes in each injection series.

### **2.13 Cell culture**

The rhabdomyosarcoma RD cells (ATCC, LGC Standards GmbH, Wesel, Germany) were routinely cultured in Dulbecco's Modified Eagle Medium DMEM containing 4.5 g/l glucose (PAA Laboratories GmbH, Germany), supplemented with 10% fetal bovine serum (PAA Laboratories GmbH, Germany), 100 U/ml penicillin and 100 µg/ml streptomycin (PAA Laboratories GmbH, Germany).

The human embryonic kidney cells (HEK293) (ATCC, LGC Standards GmbH, Wesel, Germany) were cultured in Dulbecco's Modified Eagle Medium DMEM containing 4.5 g/l glucose (Gibco, Life Technologies GmbH, Darmstadt, Germany), supplemented with 2 mM L-glutamine (PAA Laboratories GmbH, Germany), 10% fetal bovine serum (PAA Laboratories GmbH, Germany), 100 U/ml penicillin and 100 µg/ml streptomycin (PAA Laboratories GmbH, Germany).

The RD and HEK293 cells were maintained in the culture flasks at 37°C in a humidified atmosphere of 5% CO<sub>2</sub>. 80-90% confluent cells were splitted using 0.25% Trypsin-EDTA solution (Life Technologies GmbH, Darmstadt, Germany). For the experiments, the cells were seeded into 6-well plates (BD Biosciences, Franklin Lakes, NJ, USA) at the density  $0.2 \times 10^6$  cells / well. The cells were cultured overnight at 37°C in a humidified atmosphere of 5% CO<sub>2</sub> to allow them to attach. After attachment, the cells were treated for 24 hours with 10 µM B-RAF inhibitor PLX-4720 (Selleck Chemicals, Houston, TX, USA) dissolved in DMSO (50 mM as a stock). Equal amounts of DMSO (Carl Roth, Karlsruhe, Germany) were used as a control.

## **2.14 Data analysis**

Data are provided as means  $\pm$ SEM, n represents the number of independent experiments or number of *Xenopus* oocytes investigated. All oocytes experiments were repeated with at least 3 batches of oocytes. In all repetitions, qualitatively similar data were obtained. Results were tested for significance by using non-parametric Kruskal-Wallis test, unpaired Student's t-test or Mann-Whitney test, where appropriate. Only results with  $p < 0.05$  were considered statistically significant. All statistical analysis was performed with GraphPad InStat version 3.0 (GraphPad Software, La Jolla, California, USA).

## 3 Results

### 3.1 B-RAF regulates hERG channels

#### 3.1.1 Wild-type B-RAF stimulates the hERG-mediated current in *Xenopus* oocytes

cRNA encoding hERG was injected either alone or together with cRNA encoding human wild-type B-RAF in *Xenopus* oocytes. As a control, the same amount of water was injected in *Xenopus* oocytes. The hERG-mediated currents were determined utilizing a dual-electrode voltage clamp and the channel activity was analyzed by depolarization from -80 mV holding potential to different voltages followed by a 500 ms pulse to -60 mV. As illustrated in Figure 11, the tail current following the injection of water in *Xenopus* oocytes was low in comparison with *Xenopus* oocytes injected with cRNA encoding hERG. Thus, *Xenopus* oocytes express low levels of channels displaying tail currents similar to those of hERG channels. However, strong tail currents were observed following the injection of cRNA encoding hERG in *Xenopus* oocytes. The hERG-mediated currents were significantly enhanced by additional co-expression of wild-type B-RAF in hERG-expressing *Xenopus* oocytes.

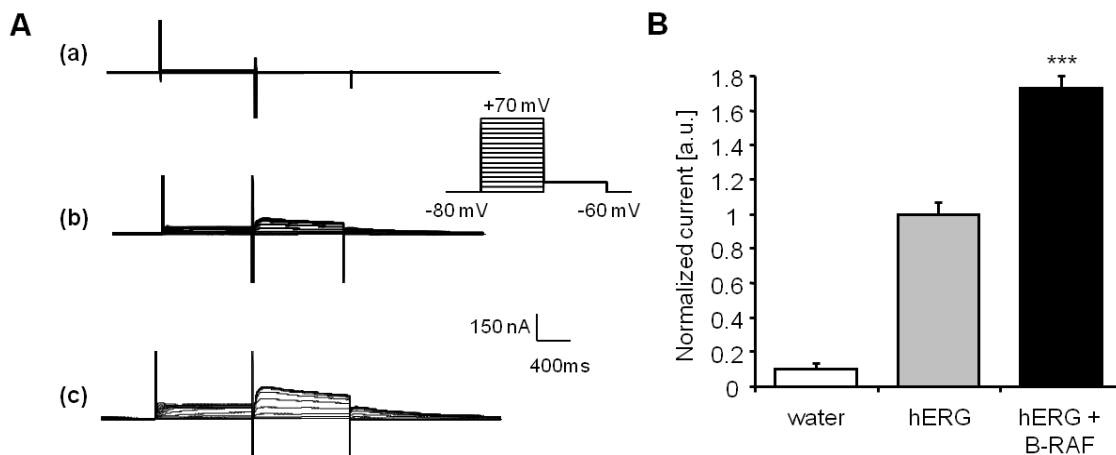


**Figure 11:** Coexpression of B-RAF increased the hERG current in *Xenopus* oocytes. The *Xenopus* oocytes were depolarized from -80 mV holding potential to different voltages followed by a 500 ms repolarization to -60 mV evoking outward tail currents. A. Original tracings recorded in *Xenopus* oocytes injected with water (a), with cRNA en-

coding hERG alone (b) or with cRNA encoding hERG together with wild-type B-RAF (c). B. Arithmetic means  $\pm$ SEM ( $n = 12-47$ , arbitrary units) of the normalized outward tail current following a depolarization to +70 mV, recorded in *Xenopus* oocytes injected with water (white bar), with cRNA encoding hERG alone (light grey bar), or with cRNA encoding both, hERG and wild-type B-RAF (black bar). \*\*\* ( $p < 0.001$ ) indicates statistically significant difference from *Xenopus* oocytes expressing hERG channels alone

### 3.1.2 The current-voltage relationship of hERG currents with or without co-expression of wild-type B-RAF

The amplitude of the peak tail current was plotted as a function of the preceding test preconditioning potential. As shown in Figure 12 A, the absolute current values were up-regulated by co-expression of wild-type B-RAF. Following normalization to the maximum peak tail current for each group, no significant kinetics differences were apparent between *Xenopus* oocytes expressing hERG together with wild-type B-RAF and *Xenopus* oocytes expressing hERG alone (Figure 12 B). In other words, the voltage required for the half maximal peak tail currents, as well as the activation threshold were similar in *Xenopus* oocytes expressing hERG alone and in *Xenopus* oocytes expressing hERG together with wild-type B-RAF.

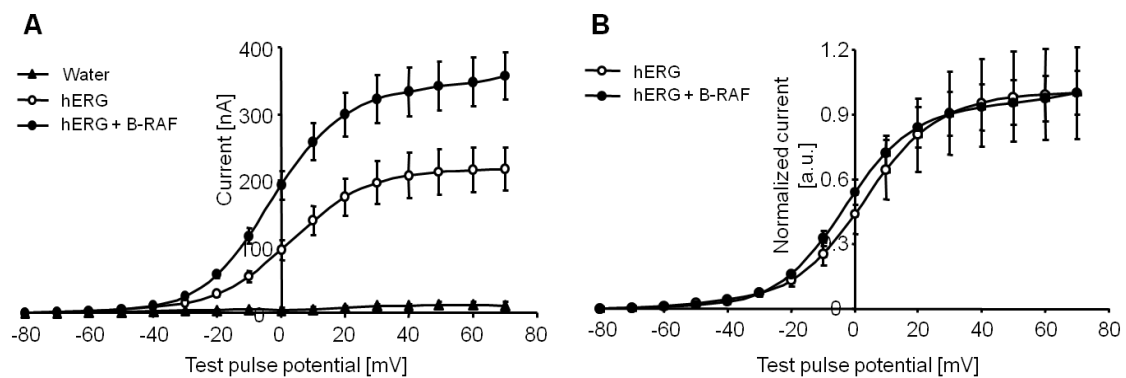


**Figure 12:** The current-voltage relationship of hERG currents with or without co-expression of wild-type B-RAF. A. Arithmetic means  $\pm$  SEM ( $n = 12-47$ , nA) of the peak tail current as a function of voltage in *Xenopus* oocytes injected with water (black triangles), with cRNA encoding hERG alone (white circles) or with cRNA encoding hERG and wild-type B-RAF (black circles). B. Arithmetic means  $\pm$ SEM ( $n = 22-47$ , arbitrary units) of the normalized peak tail current as a function of voltage in *Xenopus* oocytes injected with cRNA encoding hERG alone (white circles) or with cRNA encoding hERG together with wild-type B-RAF (black circles)

### 3.1.3 Co-expression of wild-type B-RAF increases the hERG-HA protein abundance in the cell membrane

At least in theory, B-RAF could up-regulate the hERG activity by increasing hERG channel protein abundance in the *Xenopus* oocytes plasma membrane. In order to test that possibility, immunocytochemistry and confocal microscopy were applied to visualize the hERG-HA protein in the cell membrane. As shown in Figure 13 A, the co-expression of hERG-HA with wild-type B-RAF was followed by an increase of hERG-HA protein abundance within the *Xenopus* oocyte cell membrane as compared to *Xenopus* oocytes expressing hERG-HA alone. In order to quantify the hERG-HA protein abundance in the cell membrane of *Xenopus* oocytes, chemiluminescence was employed. As compared to *Xenopus* oocytes expressing hERG-HA alone, the co-expression of wild-type B-RAF was followed by a statistically significant increase of chemiluminescence reflecting the hERG-HA protein abundance within the *Xenopus* oocyte cell membrane (Figure 13 B).

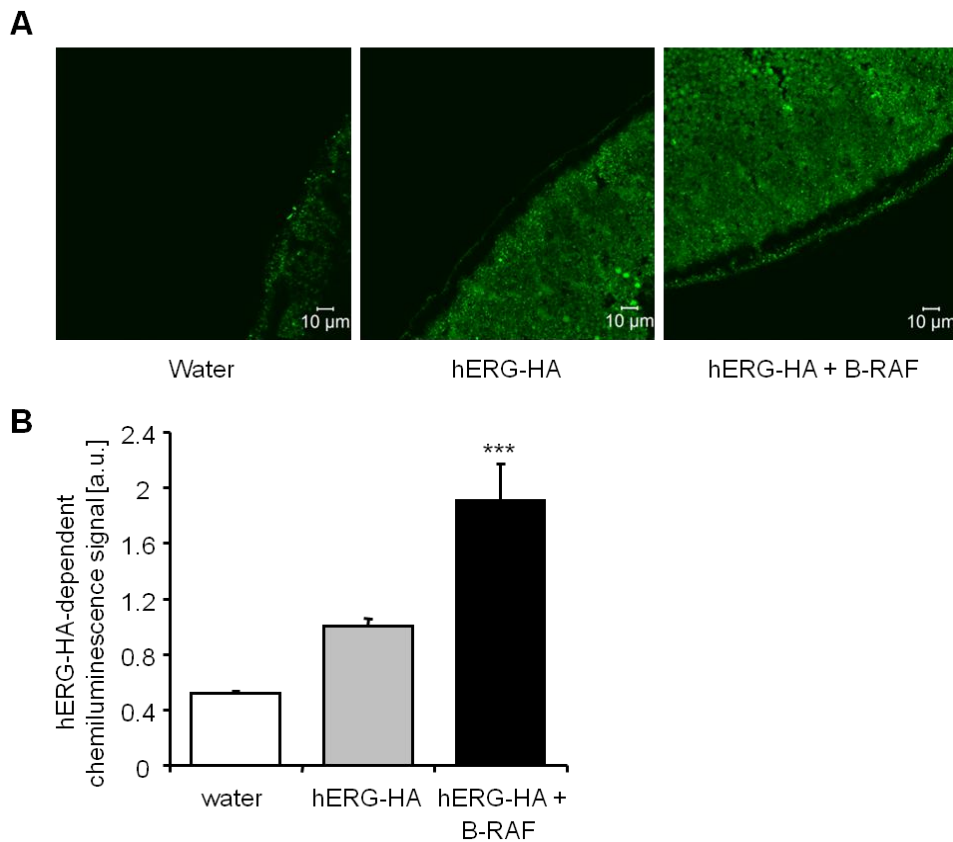


**Figure 13:** Coexpression of B-RAF increased hERG-HA protein abundance at the surface of hERG-expressing *Xenopus* oocytes. A. Confocal images of hERG-HA protein



cell surface expression in *Xenopus* oocytes injected with water (left panel), with cRNA encoding hERG-HA alone (middle panel) or with cRNA encoding hERG-HA together with wild-type B-RAF (right panel). Images are representative of three independent experiments. B. Arithmetic means  $\pm$ SEM ( $n = 81-93$ , arbitrary units) of hERG-HA protein abundance in the cell membrane measured by chemiluminescence in *Xenopus* oocytes injected with water (white bar), with cRNA encoding hERG-HA alone (light grey bar), or cRNA encoding hERG-HA and wild-type B-RAF (black bar). \*\*\* ( $p < 0.001$ ) indicates statistically significant difference from *Xenopus* oocytes expressing hERG channels alone

### 3.1.4 Effect of the B-RAF inhibitor PLX-4720 on the hERG-mediated current

Further experiments elucidated the effect of the potent B-RAF inhibitor PLX-4720 on the hERG-mediated current in B-RAF- and hERG-expressing *Xenopus* oocytes. As illustrated in Figure 14, the hERG tail current in *Xenopus* oocytes expressing both, hERG and B-RAF, was significantly decreased by a treatment with 10  $\mu$ M of the B-RAF inhibitor PLX-4720 for 24 hours. No statistically significant difference was observed between the hERG tail currents in *Xenopus* oocytes co-expressing hERG together with B-RAF and treated with 10  $\mu$ M PLX-4720 and *Xenopus* oocytes expressing hERG alone.

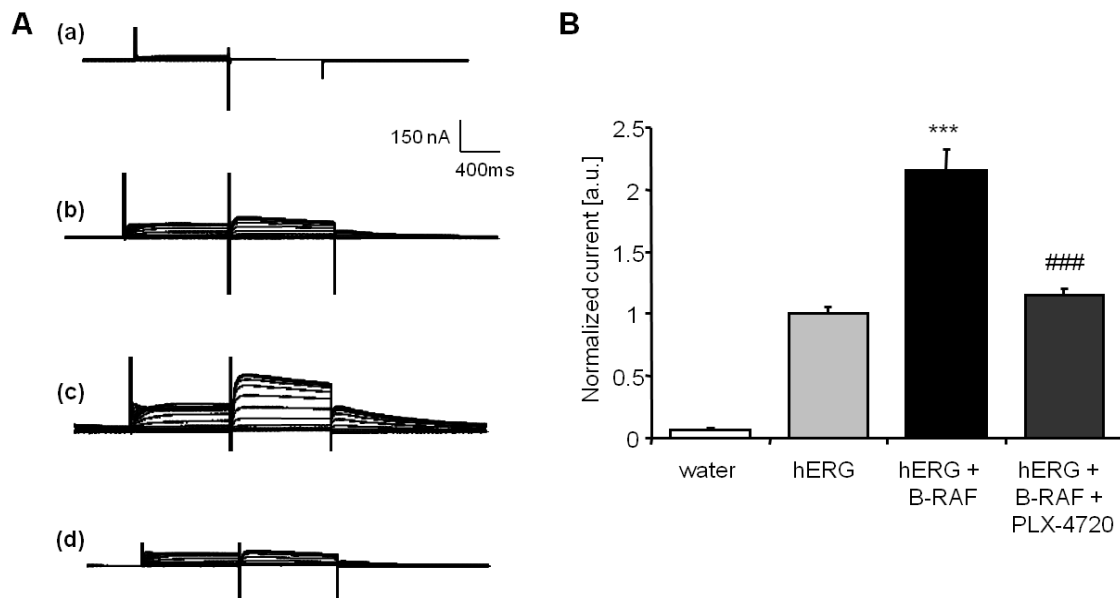


**Figure 14:** B-RAF inhibitor PLX-4720 decreased hERG current in *Xenopus* oocytes co-expressing hERG and B-RAF. The *Xenopus* oocytes were depolarized from -80 mV holding potential to different voltages followed by a 500 ms repolarization to -60 mV evoking outward tail currents. A. Original tracings recorded in *Xenopus* oocytes injected with water (a), with cRNA encoding hERG alone (b) or with cRNA encoding

hERG together with wild-type B-RAF without (c) and with (d) treatment with B-RAF inhibitor PLX-4720 (10  $\mu$ M, 24 hours). B. Arithmetic means  $\pm$ SEM (n = 12-46, arbitrary units) of the normalized outward tail current following a depolarization to +70 mV, recorded in *Xenopus* oocytes injected with water (white bar), with cRNA encoding hERG alone (light grey bar), or with cRNA encoding hERG together with wild-type B-RAF without (black bar) and with (dark grey bar) treatment with B-RAF inhibitor PLX-4720 (10  $\mu$ M, 24 hours). \*\*\* (p < 0.001) indicates statistically significant difference from *Xenopus* oocytes expressing hERG channels alone; ### (p < 0.001) indicates statistically significant difference from *Xenopus* oocytes expressing hERG together with B-RAF without treatment with PLX-4720

### 3.1.5 Effect of the B-RAF inhibitor PLX-4720 on the hERG-HA cell surface protein abundance in *Xenopus* oocytes

Figure 15 illustrates that treatment of hERG-HA and B-RAF expressing oocytes with 10  $\mu$ M PLX-4720 was followed by a decreased hERG-HA cell surface protein abundance. Thus, PLX-4720 treatment fully reversed the effect of B-RAF on hERG cell surface protein expression and activity.

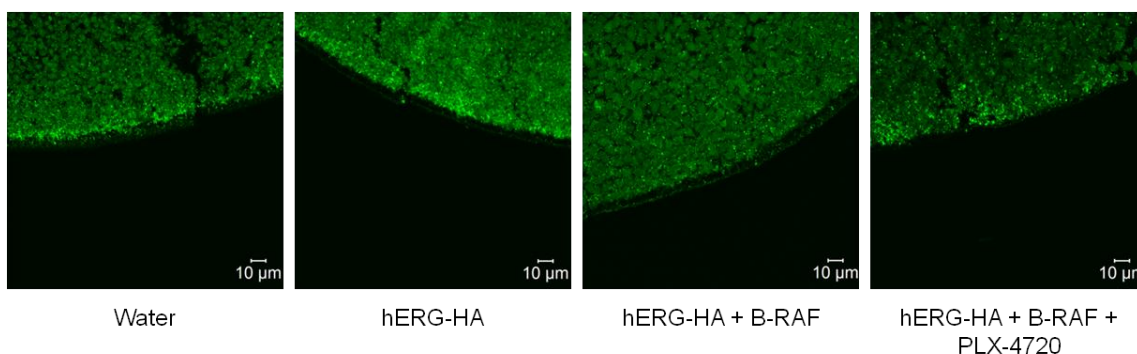


**Figure 15:** B-RAF inhibitor PLX-4720 decreases hERG-HA cell surface protein abundance. Confocal images of hERG-HA protein cell surface expression in *Xenopus* oocytes injected with water (first panel), with cRNA encoding hERG-HA alone (second panel) or with cRNA encoding hERG-HA together with wild-type B-RAF without (third panel) or with (last panel) treatment with B-RAF inhibitor PLX-4720 (10  $\mu$ M, 24 hours). Images are representative of three independent experiments

### 3.1.6 Effect of the B-RAF inhibitor PLX-4720 on the hERG cell membrane protein abundance in rhabdomyosarcoma RD cells

Another series of experiments was conducted to explore whether B-RAF similarly regulates the activity of the human ether-a-go-go related gene K<sup>+</sup> channels (hERG) in the rhabdomyosarcoma RD cells, which have previously been shown

to express hERG channels (65, 114). To this end, the rhabdomyosarcoma RD cells were treated for 24 hours with 10  $\mu$ M of the B-RAF inhibitor PLX-4720 and the hERG cell membrane protein abundance was analysed by biotinylation of the cell surface proteins with subsequent western blotting. As shown in Figure 16, the treatment of the rhabdomyosarcoma RD cells with the B-RAF inhibitor PLX-4720 was followed by a statistically significant decrease of the hERG cell membrane protein abundance as compared to the rhabdomyosarcoma RD cells treated with vehicle alone.

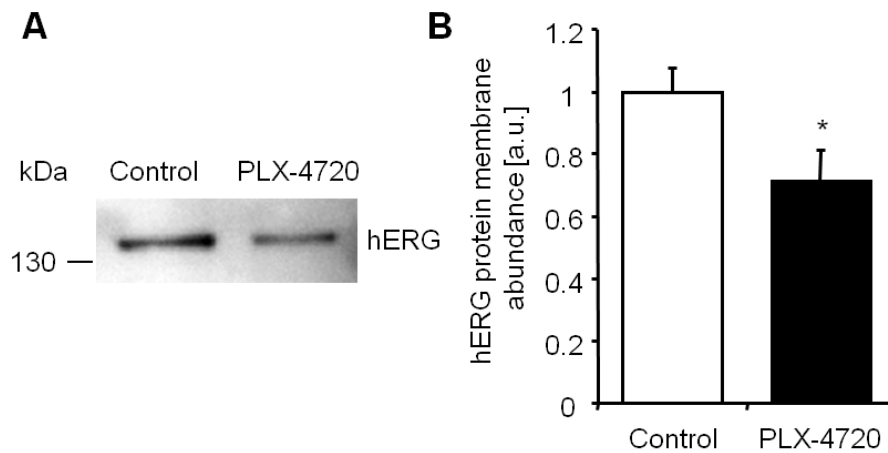


**Figure 16:** B-RAF inhibitor PLX-4720 decreased hERG protein abundance at the cell surface in the rhabdomyosarcoma RD cells. A. Representative original western blot showing hERG membrane protein abundance analyzed by cell surface biotinylation in rhabdomyosarcoma RD cells after 24 hours treatment with vehicle alone (Control) or with 10  $\mu$ M B-RAF inhibitor PLX-4720 (PLX-4720). B. Arithmetic means  $\pm$ SEM (n = 7, arbitrary units) of normalized hERG membrane protein abundance analyzed by cell surface biotinylation in the rhabdomyosarcoma RD cells after 24 hours treatment with vehicle alone (white bar) or with 10  $\mu$ M B-RAF inhibitor PLX-4720 (black bar). \*(p < 0.05) indicates statistically significant difference from rhabdomyosarcoma RD cells treated with vehicle alone

### 3.1.7 B-RAF inhibitor PLX-4720 decreases hERG cell membrane protein abundance in rhabdomyosarcoma RD cells

The rhabdomyosarcoma RD cells were treated for 24 hours with 10  $\mu$ M of the B-RAF inhibitor PLX-4720 and the hERG cell membrane protein abundance was analysed by flow cytometry experiments. As shown in Figure 17, the number of hERG-FITC positive cells, i.e. rhabdomyosarcoma RD cells expressing hERG K<sup>+</sup> channels at the cell surface, was significantly decreased following the

treatment with PLX-4720. Thus, PLX-4720 treatment decreased the hERG cell membrane protein abundance in the rhabdomyosarcoma RD cells.

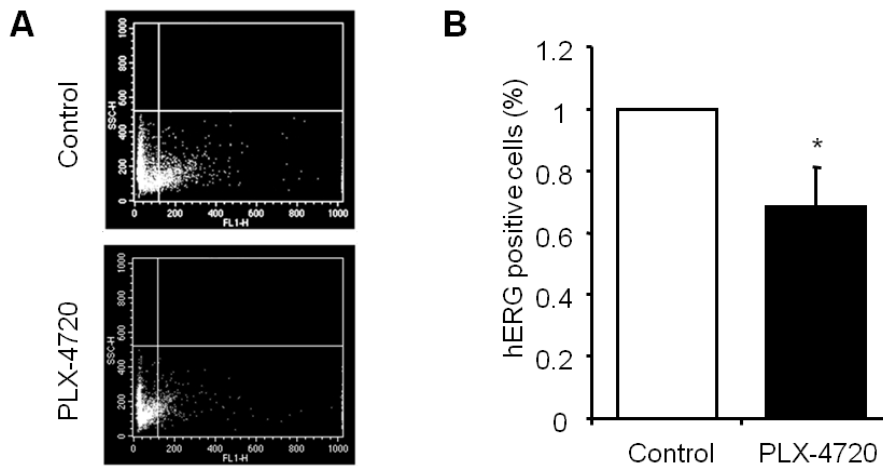


**Figure 17:** B-RAF inhibitor PLX-4720 decreased hERG protein abundance at the cell surface in the rhabdomyosarcoma RD cells. A. Representative original dot plots of hERG-FITC positive cells at the cell surface analysed by flow cytometry in rhabdomyosarcoma RD cells after 24 hours treatment with vehicle alone (Control) or with 10  $\mu$ M B-RAF inhibitor PLX-4720 (PLX-4720); FL-1 Height: hERG-FITC fluorescence intensity. B. Arithmetic means  $\pm$ SEM (n = 5, %) of normalized percentage of positive cells showing hERG expression at the cell surface analyzed by flow cytometry in the rhabdomyosarcoma RD cells after 24 hours treatment with vehicle alone (white bar) or with 10  $\mu$ M B-RAF inhibitor PLX-4720 (black bar). \*(p < 0.05) indicates statistically significant difference from rhabdomyosarcoma RD cells treated with vehicle alone

### 3.1.8 B-RAF inhibitor PLX-4720 decreases the hERG-mediated tail currents in rhabdomyosarcoma RD cells

Similar observations were made with patch clamp experiments in rhabdomyosarcoma RD cells. As illustrated in Figure 18, tail currents typical for hERG K<sup>+</sup> channels were indeed observed in rhabdomyosarcoma RD cells. The hERG-mediated tail currents were significantly lower in the rhabdomyosarcoma RD cells treated for 24 hours with 10  $\mu$ M PLX-4720 than in the rhabdomyosarcoma RD cells treated with vehicle alone.

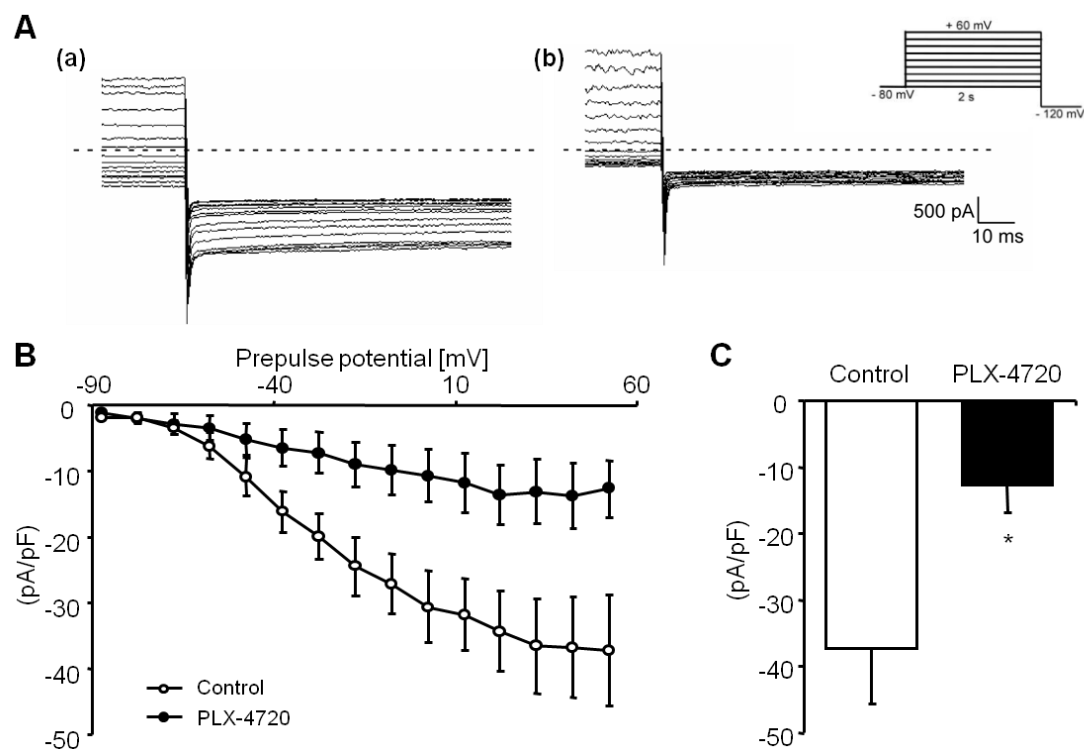


**Figure 18:** B-RAF inhibitor PLX4720 decreased hERG currents in rhabdomyosarcoma RD cells. A. Inward currents elicited in a bath solution containing 40 mM KCl according to the shown protocol: the membrane potential was held at -80 mV and then after the preconditioning step from -80 mV to +60 mV for 2 s stepped to the test potential of -120 mV for 500 ms. The currents were measured in the rhabdomyosarcoma RD cells after 24 hours treatment with vehicle alone (a) or with 10  $\mu$ M B-RAF inhibitor PLX-4720 (b). B. Mean peak current density  $\pm$ SEM (n = 5-12) plotted against the precondition potential in rhabdomyosarcoma RD cells after 24 hours treatment with vehicle alone (white cycles) or with 10  $\mu$ M B-RAF inhibitor PLX-4720 (black cycles). C. Mean peak current density  $\pm$ SEM (n = 5-12) measured at -120 mV after the precondition potential to +50 mV in rhabdomyosarcoma RD cells after 24 hours treatment with vehicle alone (white bar) or with 10  $\mu$ M B-RAF inhibitor PLX-4720 (black bar). \*(p < 0.05) indicates statistically significant difference from rhabdomyosarcoma RD cells treated with vehicle alone

## 3.2 B-RAF regulates the sodium-coupled glucose transporter SGLT1

### 3.2.1 Wild-type B-RAF stimulates the SGLT1 mediated electrogenic glucose transport

The carrier was expressed in *Xenopus* oocytes with or without additional expression of the kinase. The glucose transport was estimated from the current generated following addition of substrate to the bath solution. The current was

determined utilizing a dual electrode voltage clamp. The addition of glucose (10 mM) to the extracellular fluid did not induce an appreciable inward current in water-injected *Xenopus* oocytes, indicating that *Xenopus* oocytes do not express appreciable endogenous electrogenic glucose transport (Figure 19). In *Xenopus* oocytes expressing SGLT1, however, glucose (10 mM) induced an inward current ( $I_g$ ) reflecting electrogenic entry of  $\text{Na}^+$  and glucose. As illustrated in Figure 19,  $I_g$  was significantly enhanced by additional coexpression of B-RAF.

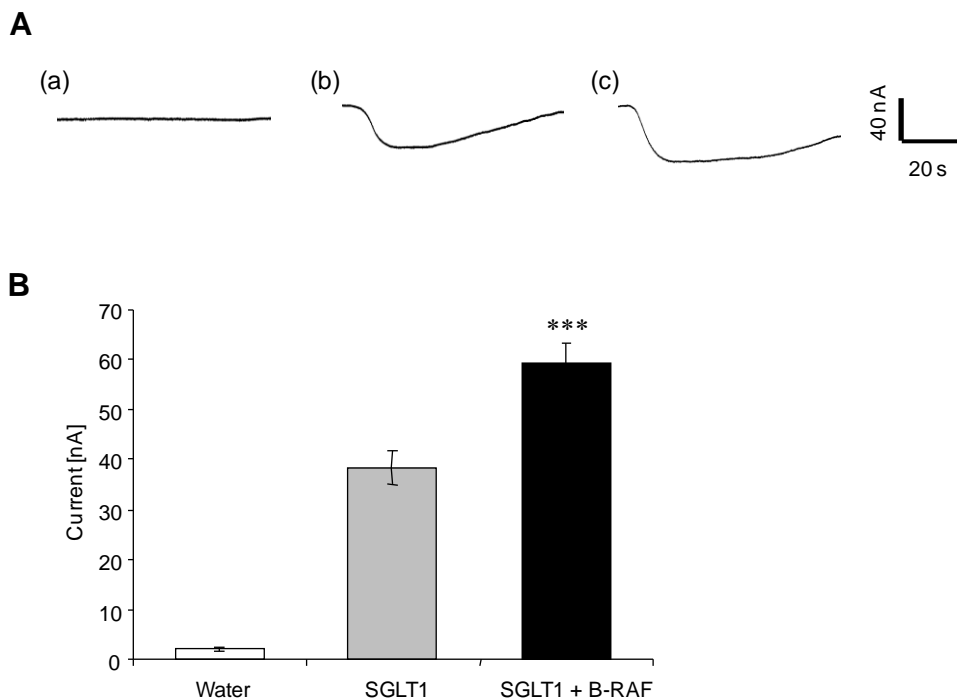


**Figure 19:** Coexpression of B-RAF increases electrogenic glucose transport in SGLT1-expressing *Xenopus* oocytes. A. Representative original tracings showing glucose-induced current (10 mM) ( $I_g$ ) in *Xenopus* oocytes injected with water (a), expressing SGLT1 without (b) or with additional coexpression of wild-type B-RAF (c). B. Arithmetic means  $\pm$ SEM (n =11-14, nA) of glucose (10 mM)-induced current ( $I_g$ ) in *Xenopus* oocytes injected with water (water, white bar), expressing SGLT1 without (SGLT1, grey bar) or with additional coexpression of wild-type B-RAF (SGLT1+B-RAF, black bar). \*\*\*( $p < 0.001$ ) indicates statistically significant difference from *Xenopus* oocytes expressing SGLT1 alone

### 3.2.2 B-RAF enhanced the maximal current

The kinetic analysis of the glucose-induced currents in SGLT1-expressing *Xenopus* oocytes (Figure 20) yielded a maximal  $I_g$  of  $58.8 \pm 2.3$  nA (n = 8). The

coexpression of B-RAF significantly enhanced the maximal  $I_g$  to  $82.0 \pm 0.6$  nA ( $n = 8$ ). The calculation of the glucose concentration required for half maximal  $I_g$  ( $K_M$ ) yielded values of  $425 \pm 77$   $\mu$ M ( $n = 8$ ) in oocytes expressing SGLT1 alone and of  $288 \pm 88$   $\mu$ M ( $n = 8$ ) in the oocytes expressing SGLT1 together with B-RAF, which are not significantly different. Accordingly, the coexpression of B-RAF enhanced the SGLT1 activity at least in part by increasing the maximal current.

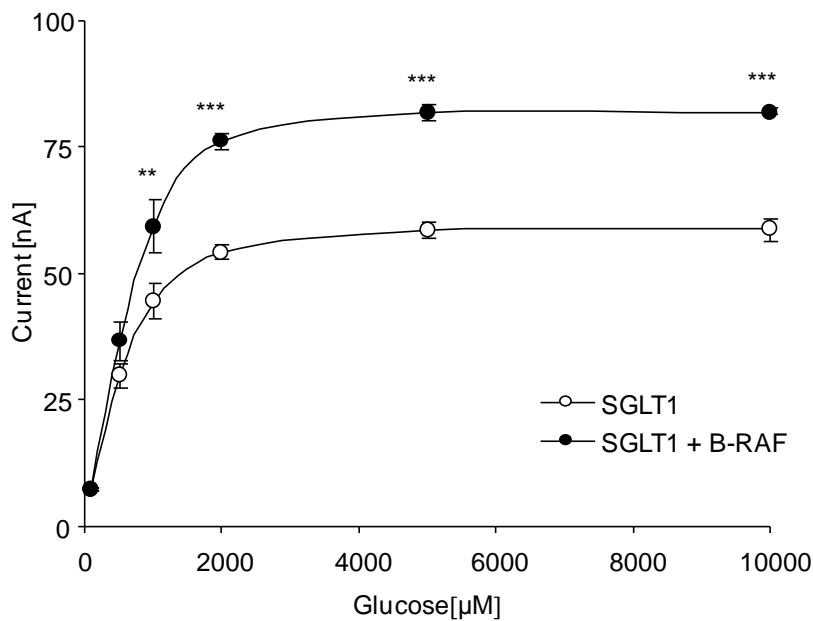


**Figure 20:** Coexpression of B-RAF increases maximal glucose transport rate in SGLT1-expressing *Xenopus* oocytes. Arithmetic means  $\pm$ SEM ( $n = 6$ , nA) of glucose induced current ( $I_p$ ) as a function of glucose concentration in *Xenopus* oocytes expressing SGLT1 without (open circles) and with additional coexpression of wild-type B-RAF (closed circles). \*\* ( $p < 0.01$ ), \*\*\* ( $p < 0.001$ ) indicates statistically significant difference from *Xenopus* oocytes expressing SGLT1 alone at every glucose concentration applied

### 3.2.3 B-RAF increases the SGLT1 protein abundance in the cell membrane

An enhanced SGLT1 activity could result from increased carrier protein abundance in the plasma membrane. To test this possibility, immunocytochemistry and confocal microscopy were employed to quantify the SGLT1 protein abundance in the cell membrane. As illustrated in Figure 21 A, the coexpression of B-RAF was followed by an increase of SGLT1 protein abundance within the oocyte cell membrane. The protein abundance was quantified utilizing chemilumi-

nescence experiments. As shown in Figure 21 B, the coexpression of B-RAF was again followed by a significant increase of cell membrane SGLT1 protein abundance.

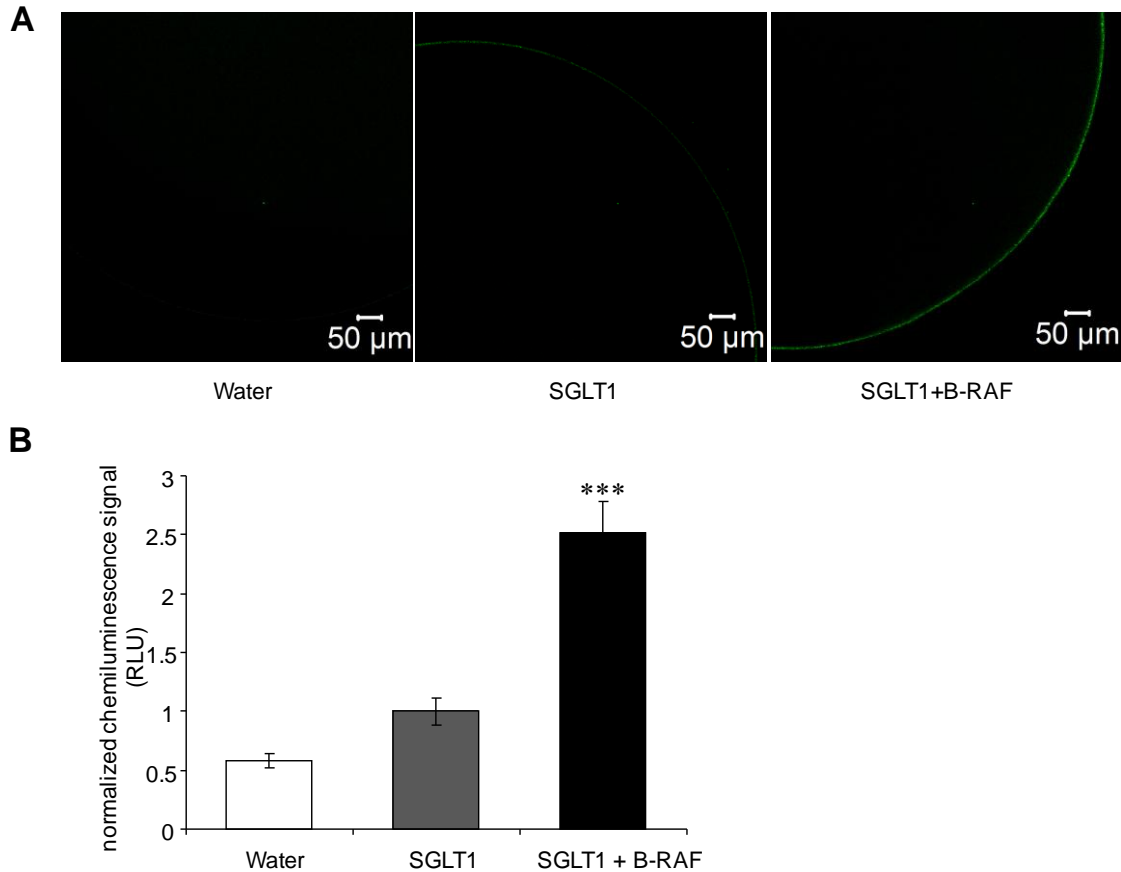


**Figure 21:** Coexpression of B-RAF enhanced SGLT1 protein abundance at the cell surface in SGLT1-expressing *Xenopus* oocytes. A. Confocal images reflecting the SGLT1 membrane protein abundance in *Xenopus* oocytes injected with water (water), expressing SGLT1 without (SGLT1) or with additional coexpression of wild-type B-RAF (SGLT1+B-RAF). The images are representative of three independent experiments. B. Arithmetic means  $\pm$ SEM ( $n = 43-47$ , arbitrary units) of the chemiluminescence of SGLT1 protein abundance in *Xenopus* oocytes injected with water (water), expressing SGLT1 without (SGLT1) or with additional coexpression of wild-type B-RAF (SGLT1+B-RAF), \*\*\*( $p < 0.001$ ) indicates statistically significant difference from *Xenopus* oocytes expressing SGLT1 alone



### 3.3 B-RAF regulates the sodium-coupled phosphate cotransporters NaPi-IIa and NaPi-IIb

#### 3.3.1 Wild-type B-RAF increased the electrogenic phosphate transport in NaPi-IIa-expressing *Xenopus* oocytes

The cotransporter was expressed in *Xenopus* oocytes with or without additional coexpression of wild-type B-RAF. The phosphate transport was estimated from the current generated following the addition of phosphate to the extracellular fluid. The substrate-induced current was determined utilizing a dual-electrode voltage clamp. As illustrated in Figure 22, the addition of phosphate (1 mM) to the bath solution did not induce an appreciable inward current in the water-injected *Xenopus* oocytes. Thus, *Xenopus* oocytes do not express appreciable endogenous electrogenic phosphate transporters. In *Xenopus* oocytes expressing NaPi-IIa, however, phosphate induced an inward current ( $I_P$ ) reflecting an electrogenic entry of  $\text{Na}^+$  and phosphate. As shown in Figure 22,  $I_P$  was significantly enhanced by the additional coexpression of wild-type B-RAF in NaPi-IIa-expressing *Xenopus* oocytes.

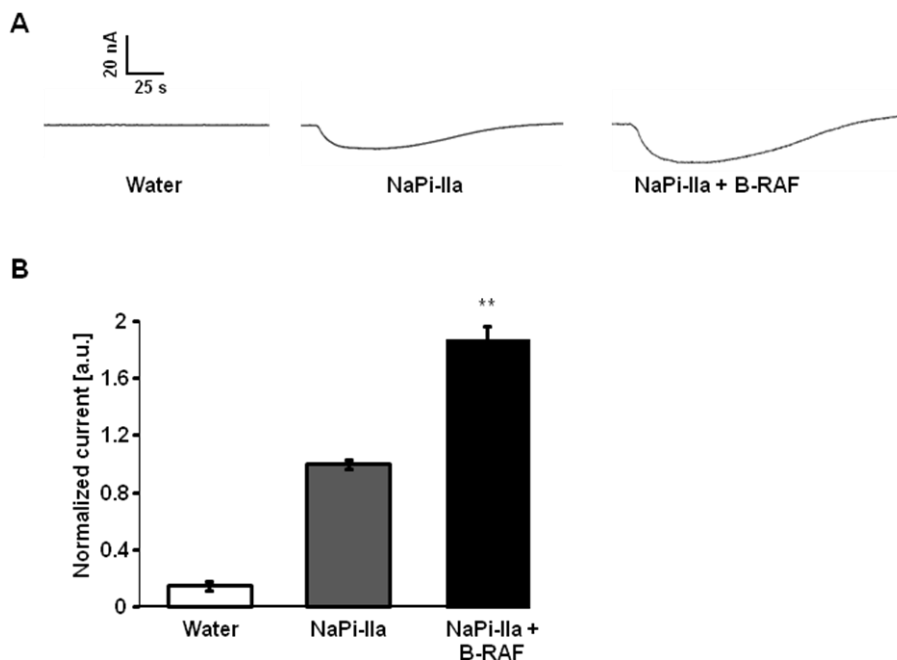


**Figure 22:** Coexpression of B-RAF increased the electrogenic phosphate transport in NaPi-IIa-expressing *Xenopus* oocytes. A. Representative original tracings showing

phosphate-induced current (1 mM) ( $I_P$ ) in *Xenopus* oocytes injected with water (Water), expressing NaPi-IIa without (NaPi-IIa) or with additional coexpression of wild-type B-RAF (NaPi-IIa + B-RAF). B. Arithmetic means  $\pm$ SEM ( $n = 14-17$ , arbitrary units) of normalized phosphate-induced current ( $I_P$ ) in *Xenopus* oocytes injected with water (white bar), expressing NaPi-IIa without (grey bar) or with additional coexpression of wild-type B-RAF (black bar). \*\* ( $p < 0.01$ ) indicates statistically significant difference from *Xenopus* oocytes expressing NaPi-IIa alone

### 3.3.2 Wild-type B-RAF increased the maximal phosphate transport rate in the NaPi-IIa-expressing *Xenopus* oocytes

B-RAF could have been effective by increasing the maximal transport rate or by enhancing the affinity of the carrier. To distinguish between these two possibilities, a kinetic analysis of the phosphate-induced currents was performed. As shown in Figure 23, the phosphate transport was saturable at increasing substrate concentrations. The kinetic analysis yielded a maximal  $I_P$  of  $16.25 \pm 0.12$  nA ( $n = 12$ ) in the *Xenopus* oocytes expressing NaPi-IIa alone. The coexpression of wild-type B-RAF significantly enhanced the maximal  $I_P$  to  $29.09 \pm 0.30$  nA ( $n = 12$ ). The calculation of the phosphate concentration required for half maximal  $I_P$  ( $K_m$ ) yielded values of  $1046.61 \pm 43.96$   $\mu$ M ( $n = 12$ ) in *Xenopus* oocytes expressing NaPi-IIa alone and of  $785.60 \pm 21.94$   $\mu$ M ( $n = 12$ ) in *Xenopus* oocytes expressing NaPi-IIa together with B-RAF, the values were again significantly different. As a result, coexpression of wild-type B-RAF enhanced the NaPi-IIa activity by increasing the maximal current and by enhancing the affinity of the carrier.

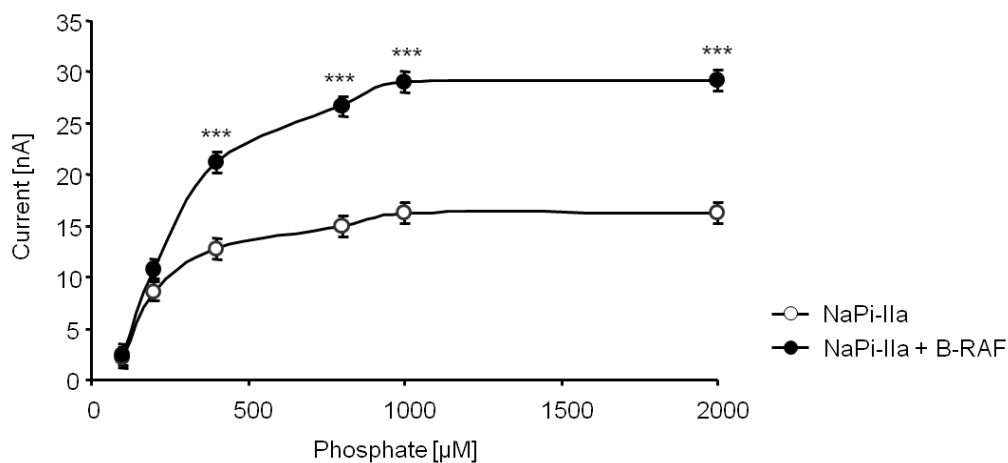


**Figure 23:** Coexpression of B-RAF increased the maximal phosphate transport rate in NaPi-IIa-expressing *Xenopus* oocytes. Arithmetic means  $\pm$ SEM ( $n = 12$ , nA) of phos-

phate-induced current ( $I_p$ ) as a function of phosphate concentration in *Xenopus* oocytes expressing NaPi-IIa without (open circles) and with additional coexpression of wild-type B-RAF (closed circles). \*\*\* ( $p < 0.001$ ) indicates statistically significant difference from *Xenopus* oocytes expressing NaPi-IIa alone at the respective phosphate concentrations

### 3.3.3 Wild-type B-RAF increased the NaPi-IIa protein abundance at the cell membrane of *Xenopus* oocytes

The enhanced maximal NaPi-IIa activity could have been caused by the increased carrier protein abundance in the plasma membrane. Thus, immunocytochemistry with confocal microscopy was employed to visualize the NaPi-IIa protein abundance in the cell membrane. As shown in Figure 24 A, the coexpression of wild-type B-RAF was followed by an increase of the NaPi-IIa protein abundance within the oocytes' cell membrane. The protein abundance was quantified utilizing chemiluminescence. Figure 24 B illustrates that the coexpression of wild-type B-RAF was followed by a significant increase of chemiluminescence.

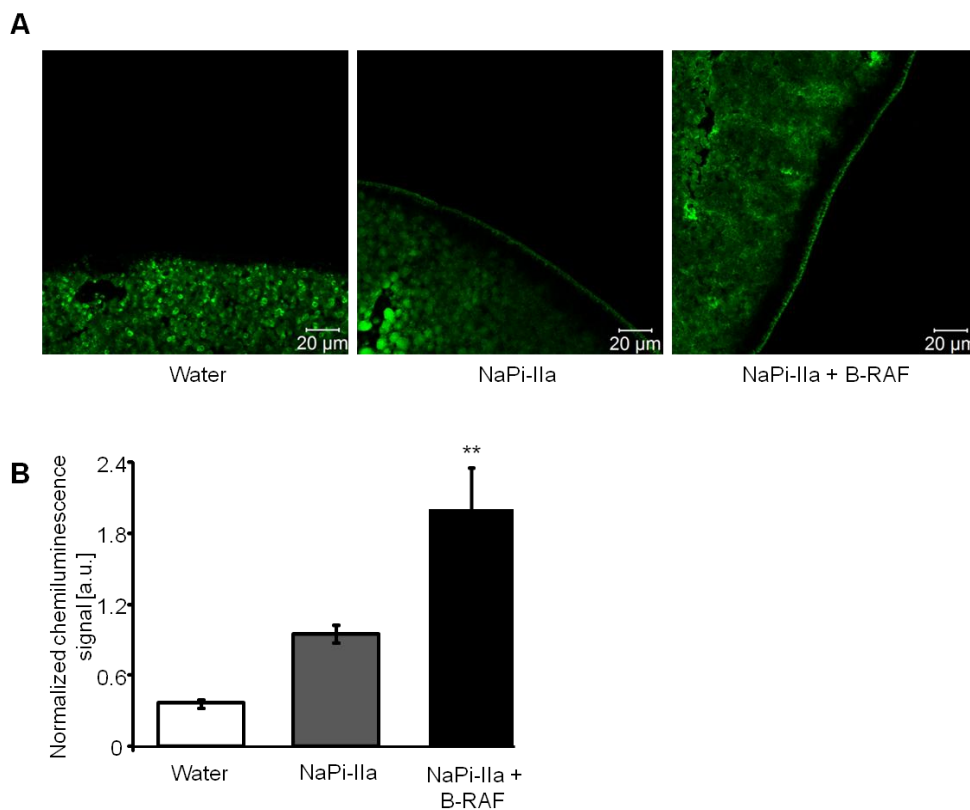


**Figure 24:** Coexpression of B-RAF enhanced the NaPi-IIa protein abundance at the cell surface in NaPi-IIa-expressing *Xenopus* oocytes. A. Confocal images reflecting NaPi-IIa

membrane protein abundance in *Xenopus* oocytes injected with water (Water), expressing NaPi-IIa without (NaPi-IIa) or with additional coexpression of wild-type B-RAF (NaPi-IIa+B-RAF). The images are representative for three independent experiments. B. Arithmetic means  $\pm$ SEM (n = 44-63, arbitrary units) of the chemiluminescence of NaPi-IIa cell surface protein abundance in *Xenopus* oocytes injected with water (white bar), expressing NaPi-IIa without (grey bar) or with additional coexpression of wild-type B-RAF (black bar). \*\* (p < 0.01) indicates statistically significant difference from *Xenopus* oocytes expressing NaPi-IIa alone

### 3.3.4 Effect of the B-RAF inhibitor PLX-4720 on NaPi-IIa protein abundance at the cell surface in HEK293 cells

Another series of experiments was conducted to explore whether B-RAF similarly regulates the protein abundance of NaPi-IIa in HEK293 cells. To this end, HEK293 cells were treated with 10  $\mu$ M of the B-RAF inhibitor PLX-4720 for 24 hours and the NaPi-IIa cell membrane protein abundance was analysed by biotinylation of the cell surface proteins with subsequent western blotting. As illustrated in Figure 25, treatment of HEK293 cells with B-RAF inhibitor PLX-4720 was followed by a statistically significant decrease in NaPi-IIa cell membrane protein abundance as compared to HEK293 cells treated with vehicle alone. Thus, PLX-4720 treatment decreased the NaPi-IIa cell membrane protein abundance in HEK293 cells.

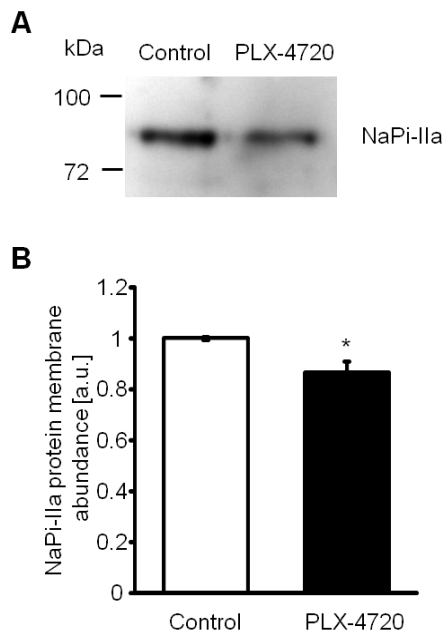


**Figure 25:** B-RAF inhibitor PLX-4720 decreased the NaPi-IIa protein abundance at the cell surface in HEK293 cells. A. Representative original western blot showing NaPi-IIa

membrane protein abundance analysed by cell surface biotinylation in HEK293 cells after 24 hours treatment with vehicle alone (Control) or with 10  $\mu\text{M}$  B-RAF inhibitor PLX-4720 (PLX-4720). B. Arithmetic means  $\pm$ SEM ( $n = 6$ , arbitrary units) of normalized NaPi-IIa membrane protein abundance analysed by cell surface biotinylation in HEK293 cells after 24 hours treatment with vehicle alone (white bar) or with 10  $\mu\text{M}$  B-RAF inhibitor PLX-4720 (black bar). \* ( $p < 0.05$ ) indicates statistically significant difference from HEK293 cells treated with vehicle alone

### 3.3.5 Wild-type B-RAF increased the electrogenic phosphate transport in NaPi-IIb-expressing *Xenopus* oocytes

Further experiments explored whether B-RAF similarly influences the activity of the related type II Na<sup>+</sup>-coupled phosphate cotransporter NaPi-IIb. As illustrated in Figure 26, addition of phosphate (1 mM) to the bath solution did not induce an appreciable inward current in the water-injected *Xenopus* oocytes. In *Xenopus* oocytes expressing NaPi-IIb, however, the phosphate induced an inward current ( $I_p$ ), which was significantly increased by additional coexpression of wild-type B-RAF.

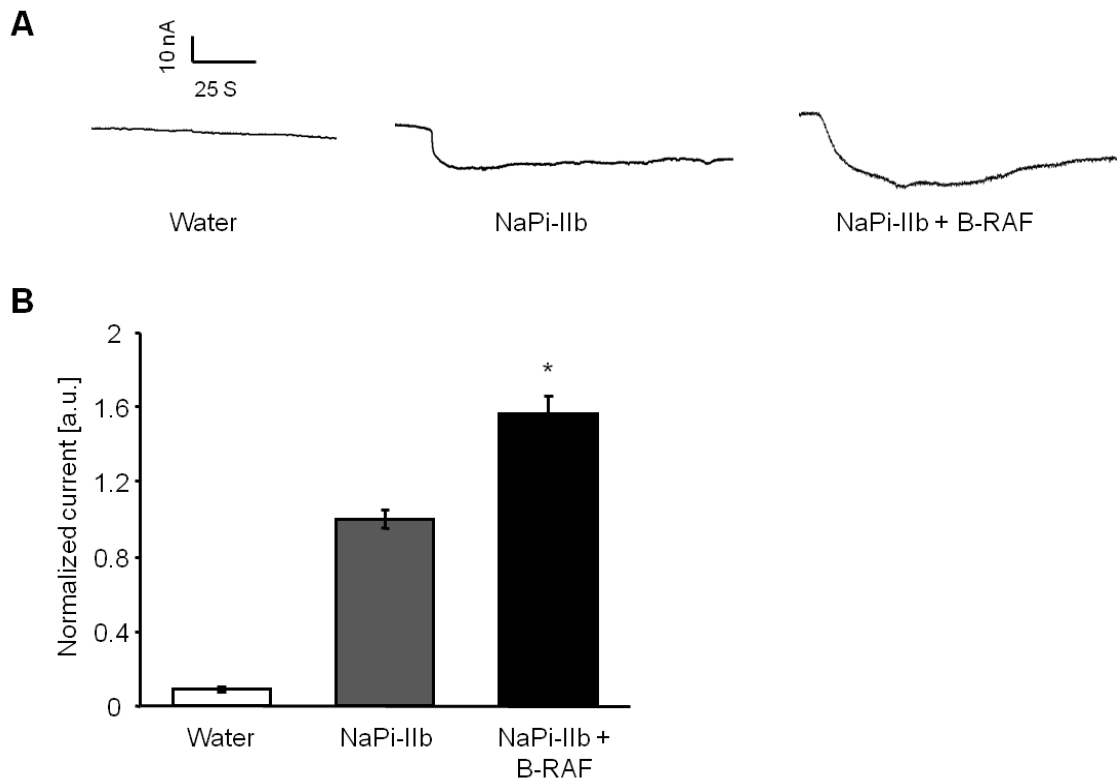


**Figure 26:** Coexpression of B-RAF increased the electrogenic phosphate transport in NaPi-IIb-expressing *Xenopus* oocytes. A. Representative original tracings showing phosphate-induced current (1 mM) ( $I_p$ ) in *Xenopus* oocytes injected with water (Water),

expressing NaPi-IIb without (NaPi-IIb) or with additional coexpression of wild-type B-RAF (NaPi-IIb + B-RAF). B. Arithmetic means  $\pm$ SEM ( $n = 14$ , arbitrary units) of normalized phosphate-induced current ( $I_p$ ) in *Xenopus* oocytes injected with water (white bar), expressing NaPi-IIb without (grey bar) or with additional coexpression of wild-type B-RAF (black bar). \* ( $p < 0.05$ ) indicates statistically significant difference from *Xenopus* oocytes expressing NaPi-IIb alone

### 3.3.6 Wild-type B-RAF increased the maximal phosphate transport rate in NaPi-IIb-expressing *Xenopus* oocytes

Figure 27 illustrates that the phosphate transport was saturable at increasing substrate concentrations. The kinetic analysis yielded a maximal  $I_p$  of  $15.45 \pm 0.80$  nA ( $n = 10$ ) in *Xenopus* oocytes expressing NaPi-IIb alone. The coexpression of wild-type B-RAF again significantly enhanced the maximal  $I_p$  to  $24.48 \pm 0.93$  nA ( $n = 8-10$ ). The calculation of the phosphate concentration required for half maximal  $I_p$  ( $K_m$ ) yielded values of  $828.96 \pm 22.83$   $\mu$ M ( $n = 10$ ) in *Xenopus* oocytes expressing NaPi-IIb alone and of  $645.40 \pm 14.03$   $\mu$ M ( $n = 8-10$ ) in *Xenopus* oocytes expressing NaPi-IIb together with B-RAF, values again significantly different. As a result, coexpression of wild-type B-RAF enhanced the NaPi-IIb activity by increasing the maximal current and by enhancing the affinity of the carrier.

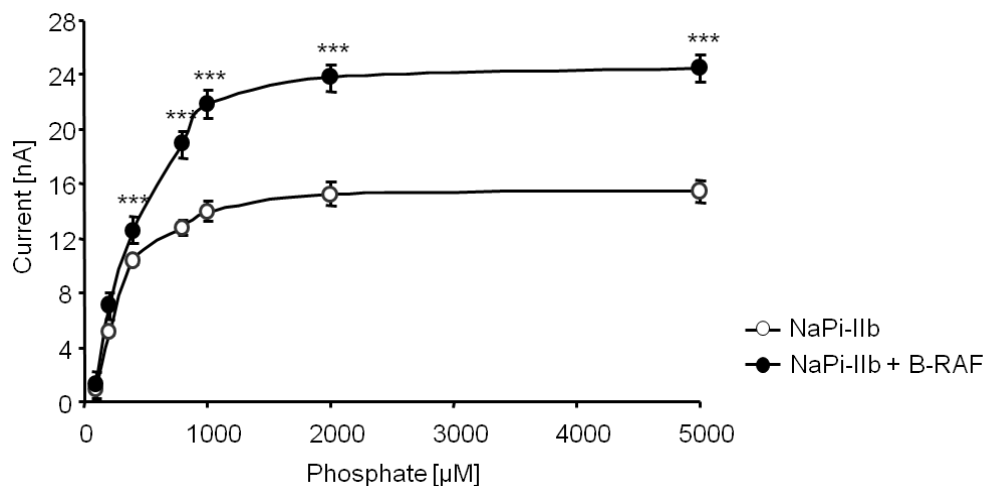


**Figure 27:** Coexpression of B-RAF increased maximal phosphate transport rate in NaPi-IIb-expressing *Xenopus* oocytes. Arithmetic means  $\pm$ SEM ( $n = 10$ , nA) of phosphate-induced current ( $I_p$ ) as a function of phosphate concentration in *Xenopus* oocytes expressing NaPi-IIb without (open circles) and with additional coexpression of wild-type B-RAF (closed circles). \*\*\* ( $p < 0.001$ ) indicates statistically significant difference from *Xenopus* oocytes expressing NaPi-IIb alone at the respective phosphate concentrations

## 4 Discussion

The data regarding the role of B-RAF in the regulation of membrane transport are limited and mainly focused on the association between mutations of B-RAF and the activity of transporters in different cancers. This study identifies a novel role of B-RAF in the regulation of ion channels and transporters.

The present work reveals that the serine/threonine kinase B-RAF is a powerful stimulator of the human ether-a-go-go related-gene K<sup>+</sup> channels (hERG). The coexpression of wild-type B-RAF increases the hERG channel protein abundance in the cell membrane and thus increases the respective hERG-mediated current across the cell membrane in *Xenopus* oocytes. Furthermore, the down-regulation of the hERG channel protein abundance and the activity in rhabdomyosarcoma RD cells, by treatment with the B-RAF inhibitor PLX-4720, points out a role of B-RAF in the regulation of hERG channels in those tumour cells (115). It must be kept in mind, though, that the selectivity of the inhibitor may be limited. The experiments in *Xenopus* oocytes show, however, that the inhibitor PLX-4720 reverses the effect of wild-type B-RAF coexpression and apparently does not influence the hERG activity by mechanisms other than B-RAF inhibition. The data obtained from *Xenopus* oocytes experiments indicate that wild-type B-RAF is at least partially effective through effects on the channel insertion into the cell membrane and/or channel protein stability in the cell membrane (115). It also can be concluded that the effects may not depend on direct phosphorylation of the channel by B-RAF, because no putative consensus sequence specific for the B-RAF phosphorylation site recognition motif could be identified in the hERG protein sequence. Instead, B-RAF may be effective by influencing other regulators of hERG channels. At least in theory, the hERG expression in the plasma membrane can be regulated by B-RAF via Nedd4-2. It was previously shown that hERG and Nedd4-2 can interact with each other. This interaction leads to ubiquitination and degradation of mature channel (116-118). Moreover, theoretically, B-RAF may be effective by influencing the activity of other kinases. The kinases involved in the effect of growth factors on the hERG expression include protein tyrosine kinases (119), VEGFR-2 (KDR) kinase (120), serum- and glucocorticoid-inducible kinase isoforms SGK1 and SGK3 (116,

121), AMP-activated protein kinase (114) and phosphatidylinositol-3-phosphate-5-kinase PIKfyve (122).

The hERG channels are also involved in the pathophysiology of cancer (70, 123, 124). Several studies indicate that hERG controls cell proliferation, cell invasiveness and tumour cell neoangiogenesis (125). Thus, B-RAF-sensitive regulation of the hERG channel may have an impact on proliferation, survival and migration of tumour cells (126, 127). The regulation of channels by coexpressed signalling molecules in *Xenopus* oocytes may not necessarily reflect the effect of the respective signalling molecule on the channel activity in tumour cells. The interaction of signalling molecules with channels may depend on the expression level of the channel and the signalling molecule, which may be different in cRNA-injected *Xenopus* oocytes and defined mammalian cells. Moreover, the additional signalling pathways expressed differently in *Xenopus* oocytes and mammalian cells may modify the interaction of the signalling molecule with the channels. The observed effect of the B-RAF inhibitor PLX-4720 strongly suggests, however, that the B-RAF sensitivity of hERG channels is relevant in rhabdomyosarcoma RD cells. Thus, B-RAF-sensitive hERG K<sup>+</sup> channel up-regulation possibly contributes to cell proliferation and apoptosis of tumour cells.

Considering the critical role of hERG K<sup>+</sup> channels in the regulation of cardiac repolarization, the up-regulation of these channels by B-RAF, at least in theory, may further influence the hERG-associated cardiac repolarization disorders (128). B-RAF is expressed in the heart. It was previously reported that this kinase is involved in the regulation of cardiomyocytes survival, growth and hypertrophy (129, 130). A negative influence of B-RAF inhibitors on cardiomyocytes function and survival may present an important potential side effect of B-RAF inhibitors (131).

This work points out that wild-type B-RAF is a powerful stimulator of the voltage-gated hERG K<sup>+</sup> channels and may as well participate in the proliferation, survival and function of tumour cells and possibly cardiomyocytes. Next the question of the role of B-RAF in the regulation of the Na<sup>+</sup>-coupled glucose transporter SGLT1 was addressed. The serine/threonine kinase B-RAF



enhanced the SGLT1 protein abundance in the cell membrane and thus increased the transport rate by this carrier. Accordingly, B-RAF significantly increased the maximal transport rate without significantly affecting the substrate affinity of the carrier (107).

SGLT1 is well known to accomplish the Na<sup>+</sup>-coupled glucose transport across the brush border of the small intestine and the proximal tubule within the kidney. The glucose transport by SGLT1 is driven by the steep electrochemical Na<sup>+</sup> gradient across the plasma membrane (72). The coupling to Na<sup>+</sup> thus allows almost complete (re)absorption of luminal glucose in intestine and kidney.

The present experiments do not attempt to define the molecular mechanism of the B-RAF dependent regulation of SGLT1. B-RAF may influence the SGLT1 activity by direct phosphorylation of the carrier or by phosphorylation of other signalling molecules, which in turn regulate SGLT1. SGLT1 is a target of several kinases including the protein kinase A (PKA) (132, 133), the protein kinase C (PKC) (134), the serum- and glucocorticoid-inducible kinase (SGK) (135), AMP-activated protein kinase (AMPK) (136) and Janus kinase JAK2 (137). Those kinases regulate the SGLT1 activity by influencing the carrier protein abundance within the plasma membrane.

Besides its well established expression and functional role in the epithelial transport, SGLT1 is expressed in a variety of tumour cells (78, 80, 138, 139). Tumour cells further take up glucose by the facilitative glucose transporter GLUT1, a carrier accomplishing the non-concentrative glucose uptake (140, 141). The very high demand of tumour cells for nutrients may, however, require the additional involvement of SGLT1 (80). The glucose uptake through passive GLUT carriers has the advantage that it does not require energy expenditure. In contrast, the Na<sup>+</sup>-coupled glucose uptake eventually requires an ATP-consuming extrusion of the cotransported Na<sup>+</sup> by the Na<sup>+</sup>/K<sup>+</sup> ATPase. The pump further replenishes the cell with K<sup>+</sup> as the SGLT1 induced depolarization leads to cellular K<sup>+</sup> loss. Without the Na<sup>+</sup>/K<sup>+</sup> ATPase activity, the SGLT1 activity would lead to a gradual dissipation of the Na<sup>+</sup> gradient and depolarization eventually resulting in cell swelling (142). SGLT1 has, however, the advantage that it is able to allow a cellular accumulation of glucose even at a decreased extracellular glucose

concentration, which impairs the glucose uptake through the facilitative glucose carriers more profoundly than Na<sup>+</sup>-coupled glucose uptake. In contrast to the facilitative glucose carriers, SGLT1 accomplishes cellular glucose uptake even at extracellular glucose concentrations far below the intracellular concentrations. The ATP needed for the extrusion of the cotransported Na<sup>+</sup> by the Na<sup>+</sup>/K<sup>+</sup> ATPase is only a fraction of the ATP generated during degradation of glucose, even if glucose is utilized only for glycolysis without oxidative metabolism (107).

These data demonstrate that B-RAF upregulates the protein abundance and activity of the Na<sup>+</sup>-coupled glucose transporter SGLT1. The stimulation of SGLT1 may allow the maintenance of the cellular glucose delivery and thus confer survival of tumour cells at low local extracellular glucose concentration.

Finally, the obtained results show that the coexpression of the wild-type serine/threonine kinase B-RAF enhances the NaPi-IIa phosphate-induced inward current ( $I_p$ ) in *Xenopus* oocytes. Furthermore, B-RAF enhances the NaPi-IIa protein abundance in the cell membrane, thus increasing the maximal electrogenic phosphate transport rate in NaPi-IIa-expressing *Xenopus* oocytes. Additionally, B-RAF significantly modifies the substrate affinity of the carrier. The down-regulation of the NaPi-IIa protein abundance at the cell surface was observed in HEK293 cells following treatment with the B-RAF inhibitor PLX-4720, an observation again pointing to a role of B-RAF in the regulation of the Na<sup>+</sup>-coupled phosphate cotransporter NaPi-IIa. However, it must be kept in mind, that the selectivity of the inhibitor may be limited. The coexpression of B-RAF similarly enhances the NaPi-IIb phosphate-induced inward current ( $I_p$ ) by increasing the maximal electrogenic phosphate transport rate and by modifying the substrate affinity of the carrier in NaPi-IIb-expressing *Xenopus* oocytes. Thus, B-RAF regulates both members of the type II Na<sup>+</sup>-coupled phosphate cotransporter family (143).

It should be noted that the present work does not directly address the molecular mechanism involved in the regulation of carrier affinity and protein abundance in the cell membrane by B-RAF as well as it does not aim to define the *in vivo* significance of the B-RAF-sensitive regulation of renal and intestinal type II Na<sup>+</sup>-coupled phosphate cotransporters. In theory, B-RAF could directly

phosphorylate the carrier or could phosphorylate other signalling molecules, which in turn modify carrier insertion and activity.

B-RAF may be inhibited by AKT (protein kinase B) (144), a kinase similarly activated by IGF1 and stimulating the transport of glucose (135, 145, 146), amino acids (147, 148),  $\text{Ca}^{2+}$  and  $\text{H}^+$  (149),  $\text{Na}^+$  (150) as well as phosphate (151, 152). Guan et al. reported that AKT phosphorylates B-RAF at multiple residues within its amino-terminal regulatory domain (153). It was also described that SGK inhibits the activity of B-RAF (154). These data indicate that crosstalk between B-RAF and other signalling pathways can be mediated by AKT and SGK. Clearly, additional experimentation will be required to define the putative role of B-RAF signalling in the regulation of renal tubular and intestinal phosphate transport.

B-RAF contributes to the pathophysiology of polycystic kidney disease (PKD), a disorder with formation of renal cysts (144). The cysts are enlarged by cAMP, which is effective by stimulating epithelial cell proliferation and transepithelial fluid secretion (144). The influence of cAMP on cell proliferation is apparently secondary to stimulation of B-RAF, as AKT-dependent inhibition of B-RAF is disrupted in PKD (144). Whether or not B-RAF is exclusively involved in the regulation of cell proliferation or, in addition, participates in the regulation of renal tubular transport of substrates, electrolytes and fluid, requires further investigation.

B-RAF increases the cell surface protein abundance and activity of the type II  $\text{Na}^+$ -coupled phosphate transporters NaPi-IIa and NaPi-IIb. The stimulation of NaPi-IIa may become relevant in polycystic kidneys disease, a disorder with increased B-RAF activity.

To conclude, this study improves our understanding of the involvement of B-RAF in the regulation of the ion channels and transporters.

## 5 Summary

B-RAF, a serine/threonine protein kinase, is an important component of the RAS/RAF/MEK/ERK signal transduction pathway, which controls cellular proliferation, survival and differentiation. This pathway plays a central role in transmitting growth factor-triggered signals. An aberrant regulation of the cascade contributes to cancer and other human diseases. There is increasing evidence that the growth factors and their signalling pathways play an important role in the regulation of ion channels. The human ether-a-go-go (hERG) channel participates in the repolarization of the cardiac action potential in the human heart. Beyond that, hERG can be considered one of the most important ion channels involved in the establishment and maintenance of neoplastic growth.

The present study explores whether B-RAF influences hERG channel expression and activity. The obtained data indicate that hERG channel activity and hERG channel protein abundance in the cell membrane are significantly increased by the coexpression of wild-type B-RAF. Moreover, treatment with the B-RAF inhibitor PLX-4720 significantly decreases the hERG-mediated current and the hERG cell surface expression in *Xenopus* oocytes as well as in rhabdomyosarcoma RD cells.

The sodium-coupled glucose transporter SGLT1 accomplishes concentrative cellular glucose uptake against a chemical glucose gradient. As tumour cells mainly utilize glucose as a fuel, their survival critically depends on their ability to accumulate glucose from the extracellular space. Several studies indicate a functional role of SGLT1 in malignant tumours. However, the mechanism accounting for the SGLT1 protein expression in tumour cells has remained ill-defined. The present study shows that the coexpression of B-RAF enhances SGLT1 activity and SGLT1 protein abundance in the *Xenopus* oocytes cell membrane.

The present study further explores whether B-RAF regulates the sodium-dependent phosphate cotransporters NaPi-IIa and NaPi-IIb. NaPi-IIa is responsible for more than 90% of the phosphate reabsorption in the proximal tubule of the nephron. The abundance of this transporter is regulated by different factors, including dietary phosphate, the parathyroid hormone, the insulin-like growth

factor IGF1 and insulin. On the other hand, B-RAF contributes to the signalling of the insulin-like growth factor IGF1. NaPi-IIb accomplishes phosphate transport in the intestine and its altered expression was detected in several cancers. The present study reveals that the coexpression of B-RAF enhances the phosphate-induced currents in NaPi-IIa and NaPi-IIb expressing *Xenopus* oocytes. Further, B-RAF increases the NaPi-IIa protein abundance in the cell membrane of *Xenopus* oocytes. Additionally, the treatment of HEK293 cells with the B-RAF inhibitor PLX-4720 significantly decreases the NaPi-IIa protein abundance.

To conclude, B-RAF is a novel regulator of the hERG channel, the SGLT1 transporter and the sodium-dependent phosphate cotransporters NaPi-IIa and NaPi-IIb and may contribute to the pathophysiology of malignancy and deranged phosphate metabolism.

## Zusammenfassung

Die Serin-/Threoninkinase B-RAF ist eine wichtige Komponente des RAS/RAF/MEK/ERK-Signalleitungspfad, der die zelluläre Proliferation, das Überleben und die Differenzierung von Zellen kontrolliert. Dieser Signalpfad spielt eine zentrale Rolle in der Signaltransduktion von Wachstumsfaktoren. Eine gestörte Regulierung der Kaskade trägt zur Bildung von Krebs und anderen Krankheiten des Menschen bei. Die Hinweise mehren sich, dass die Wachstumsfaktoren und deren Signalpfade eine wichtige Rolle bei der Regulierung von Ionenkanälen spielen. Der menschliche ether-a-go-go (hERG) Kanal ist an der Erregungsrückbildung von Aktionspotentialen des menschlichen Herzens beteiligt. Darüber hinaus kann hERG als einer der wichtigsten Ionenkanäle angesehen werden, die in der Regulation von neoplastischem Wachstum beteiligt sind.

Die vorliegende Arbeit untersucht, ob B-RAF die Expression und die Aktivität des hERG-Kanals beeinflusst. Die vorliegenden Daten zeigen, dass sich die Aktivität des hERG-Kanals und dessen Proteinmenge in der Zellmembran durch Koexpression von Wildtyp-B-RAF signifikant gesteigert werden. Umgekehrt reduziert die Behandlung mit dem B-RAF Inhibitor PLX-4720 den hERG-medierten Strom und die hERG Expression an der Zelloberfläche signifikant in *Xenopus* Oozyten sowie in Rhabdomyosarcoma RD Zellen.

Auch der Natrium-gekoppelte Glukosetransporter SGLT1 ist für das Tumorstadium wesentlich. Er kann Glukose gegen einen chemischen Glukosegradienten zellulär aufnehmen. Da Tumorzellen hauptsächlich Glukose als Energielieferant verwenden, hängt deren Überleben wesentlich von deren Fähigkeit ab Glukose aus dem extrazellulären Raum aufzunehmen. Mehrere Studien weisen auf eine Rolle von SGLT1 bei bösartigen Tumoren hin. Dennoch blieben die Mechanismen der Funktion und der Proteinexpression von SGLT1 in Tumorzellen nur unzureichend verstanden. Die vorliegende Arbeit zeigt dass die Koexpression von B-RAF sowohl die SGLT1-Aktivität als auch die Proteinmenge in der Zellmembran von *Xenopus* Oozyten erhöht.

Des Weiteren untersucht die vorliegende Arbeit, ob B-RAF die natriumabhängigen Phosphattransporter NaPi-IIa und NaPi-IIb beeinflusst.

NaPi-IIa ist für mehr als 90% der Reabsorption von Phosphat im proximalen Tubulus des Nephrons verantwortlich. Die Menge des Transportproteins wird durch verschiedene Faktoren, wie diätisches Phosphat, das Parathormon, den insulinähnlichen Wachstumsfaktor IGF1 sowie Insulin, beeinflusst. Auf der anderen Seite trägt B-RAF zur Signalübertragung des insulinähnlichen Wachstumsfaktors IGF1 bei. NaPi-IIb bewerkstelligt den Phosphattransport im Darm. Seine veränderte Expression wurde bei verschiedenen Krebsarten gefunden. Die vorliegende Arbeit zeigt dass die Koexpression von B-RAF die phosphatinduzierten Ströme in NaPi-IIa und NaPi-IIb exprimiert in *Xenopus* Oozyten erhöht. Darüber hinaus erhöht B-RAF die Menge an NaPi-IIa in der Zellmembran von *Xenopus* Oozyten. Zusätzlich reduziert die Behandlung von HEK293 Zellen mit dem B-RAF-Inhibitor PLX-4720 die Menge von NaPi-IIa Proteinen signifikant.

Zusammenfassend ist B-RAF ein neuer Regulator des hERG-Kanals, des SGLT1-Transporters und der natriumabhängigen Phosphattransporter NaPi-IIa und NaPi-IIb und trägt möglicherweise zur Pathophysiologie von Tumorerkrankung und gestörtem Phosphatstoffwechsel bei.

## 6 References

1. Jansen HW, Ruckert B, Lurz R, Bister K. Two unrelated cell-derived sequences in the genome of avian leukemia and carcinoma inducing retrovirus MH2. *The EMBO journal* 1983;2(11):1969-75.
2. Rapp UR, Goldsborough MD, Mark GE, Bonner TI, Groffen J, Reynolds FH, Jr., et al. Structure and biological activity of v-raf, a unique oncogene transduced by a retrovirus. *Proceedings of the National Academy of Sciences of the United States of America* 1983;80(14):4218-22.
3. McPhillips F, Mullen P, MacLeod KG, Sewell JM, Monia BP, Cameron DA, et al. Raf-1 is the predominant Raf isoform that mediates growth factor-stimulated growth in ovarian cancer cells. *Carcinogenesis* 2006;27(4):729-39.
4. Rapp UR, Heidecker G, Huleihel M, Cleveland JL, Choi WC, Pawson T, et al. raf family serine/threonine protein kinases in mitogen signal transduction. *Cold Spring Harbor symposia on quantitative biology* 1988;53 Pt 1:173-84.
5. Luo Z, Diaz B, Marshall MS, Avruch J. An intact Raf zinc finger is required for optimal binding to processed Ras and for ras-dependent Raf activation in situ. *Molecular and cellular biology* 1997;17(1):46-53.
6. Matallanas D, Birtwistle M, Romano D, Zebisch A, Rauch J, von Kriegsheim A, et al. Raf family kinases: old dogs have learned new tricks. *Genes & cancer* 2011;2(3):232-60.
7. Osborne JK, Zaganjor E, Cobb MH. Signal control through Raf: in sickness and in health. *Cell research* 2012;22(1):14-22.
8. Haematology AoGaCiOa. Atlas of Genetics and Cytogenetics in Oncology and Haematology.
9. Chong H, Guan KL. Regulation of Raf through phosphorylation and N terminus-C terminus interaction. *The Journal of biological chemistry* 2003;278(38):36269-76.
10. Dhillon AS, Pollock C, Steen H, Shaw PE, Mischak H, Kolch W. Cyclic AMP-dependent kinase regulates Raf-1 kinase mainly by phosphorylation of serine 259. *Molecular and cellular biology* 2002;22(10):3237-46.
11. Warne PH, Viciano PR, Downward J. Direct interaction of Ras and the amino-terminal region of Raf-1 in vitro. *Nature* 1993;364(6435):352-5.
12. Chong H, Lee J, Guan KL. Positive and negative regulation of Raf kinase activity and function by phosphorylation. *The EMBO journal* 2001;20(14):3716-27.
13. Tran NH, Wu X, Frost JA. B-Raf and Raf-1 are regulated by distinct autoregulatory mechanisms. *The Journal of biological chemistry* 2005;280(16):16244-53.



14. Mason CS, Springer CJ, Cooper RG, Superti-Furga G, Marshall CJ, Marais R. Serine and tyrosine phosphorylations cooperate in Raf-1, but not B-Raf activation. *The EMBO journal* 1999;18(8):2137-48.
15. Garnett MJ, Rana S, Paterson H, Barford D, Marais R. Wild-type and mutant B-RAF activate C-RAF through distinct mechanisms involving heterodimerization. *Molecular cell* 2005;20(6):963-9.
16. Rushworth LK, Hindley AD, O'Neill E, Kolch W. Regulation and role of Raf-1/B-Raf heterodimerization. *Molecular and cellular biology* 2006;26(6):2262-72.
17. O'Neill E, Kolch W. Conferring specificity on the ubiquitous Raf/MEK signalling pathway. *British journal of cancer* 2004;90(2):283-8.
18. Wiese S, Pei G, Karch C, Troppmair J, Holtmann B, Rapp UR, et al. Specific function of B-Raf in mediating survival of embryonic motoneurons and sensory neurons. *Nature neuroscience* 2001;4(2):137-42.
19. Wojnowski L, Stancato LF, Larner AC, Rapp UR, Zimmer A. Overlapping and specific functions of Braf and Craf-1 proto-oncogenes during mouse embryogenesis. *Mechanisms of development* 2000;91(1-2):97-104.
20. Wojnowski L, Zimmer AM, Beck TW, Hahn H, Bernal R, Rapp UR, et al. Endothelial apoptosis in Braf-deficient mice. *Nature genetics* 1997;16(3):293-7.
21. Robinson MJ, Cobb MH. Mitogen-activated protein kinase pathways. *Current opinion in cell biology* 1997;9(2):180-6.
22. Sakata N, Patel HR, Terada N, Aruffo A, Johnson GL, Gelfand EW. Selective activation of c-Jun kinase mitogen-activated protein kinase by CD40 on human B cells. *The Journal of biological chemistry* 1995;270(51):30823-8.
23. Chang F, Steelman LS, Shelton JG, Lee JT, Navolanic PM, Blalock WL, et al. Regulation of cell cycle progression and apoptosis by the Ras/Raf/MEK/ERK pathway (Review). *International journal of oncology* 2003;22(3):469-80.
24. Peyssonnaud C, Eychene A. The Raf/MEK/ERK pathway: new concepts of activation. *Biology of the cell / under the auspices of the European Cell Biology Organization* 2001;93(1-2):53-62.
25. Roberts PJ, Der CJ. Targeting the Raf-MEK-ERK mitogen-activated protein kinase cascade for the treatment of cancer. *Oncogene* 2007;26(22):3291-310.
26. Grimberg A. Mechanisms by which IGF-I may promote cancer. *Cancer biology & therapy* 2003;2(6):630-5.
27. Butt AJ, Firth SM, Baxter RC. The IGF axis and programmed cell death. *Immunology and cell biology* 1999;77(3):256-62.

28. Hatzivassiliou G, Song K, Yen I, Brandhuber BJ, Anderson DJ, Alvarado R, et al. RAF inhibitors prime wild-type RAF to activate the MAPK pathway and enhance growth. *Nature* 2010;464(7287):431-5.
29. Leicht DT, Balan V, Kaplun A, Singh-Gupta V, Kaplun L, Dobson M, et al. Raf kinases: function, regulation and role in human cancer. *Biochimica et biophysica acta* 2007;1773(8):1196-212.
30. Wellbrock C, Hurlstone A. BRAF as therapeutic target in melanoma. *Biochemical pharmacology* 2010;80(5):561-7.
31. Wan PT, Garnett MJ, Roe SM, Lee S, Niculescu-Duvaz D, Good VM, et al. Mechanism of activation of the RAF-ERK signaling pathway by oncogenic mutations of B-RAF. *Cell* 2004;116(6):855-67.
32. Davies H, Bignell GR, Cox C, Stephens P, Edkins S, Clegg S, et al. Mutations of the BRAF gene in human cancer. *Nature* 2002;417(6892):949-54.
33. Liu L, Cao Y, Chen C, Zhang X, McNabola A, Wilkie D, et al. Sorafenib blocks the RAF/MEK/ERK pathway, inhibits tumor angiogenesis, and induces tumor cell apoptosis in hepatocellular carcinoma model PLC/PRF/5. *Cancer research* 2006;66(24):11851-8.
34. Lito P, Rosen N, Solit DB. Tumor adaptation and resistance to RAF inhibitors. *Nature medicine* 2013;19(11):1401-9.
35. Karki P, Li X, Schrama D, Fliegel L. B-Raf associates with and activates the NHE1 isoform of the Na<sup>+</sup>/H<sup>+</sup> exchanger. *The Journal of biological chemistry* 2011;286(15):13096-105.
36. Grabellus F, Worm K, Schmid KW, Sheu SY. The BRAF V600E mutation in papillary thyroid carcinoma is associated with glucose transporter 1 overexpression. *Thyroid : official journal of the American Thyroid Association* 2012;22(4):377-82.
37. Yun J, Rago C, Cheong I, Pagliarini R, Angenendt P, Rajagopalan H, et al. Glucose deprivation contributes to the development of KRAS pathway mutations in tumor cells. *Science* 2009;325(5947):1555-9.
38. Choi YW, Kim HJ, Kim YH, Park SH, Chwae YJ, Lee J, et al. B-RafV600E inhibits sodium iodide symporter expression via regulation of DNA methyltransferase 1. *Experimental & molecular medicine* 2014;46:e120.
39. Riesco-Eizaguirre G, Gutierrez-Martinez P, Garcia-Cabezas MA, Nistal M, Santisteban P. The oncogene BRAF V600E is associated with a high risk of recurrence and less differentiated papillary thyroid carcinoma due to the impairment of Na<sup>+</sup>/I<sup>-</sup> targeting to the membrane. *Endocrine-related cancer* 2006;13(1):257-69.
40. Porra V, Ferraro-Peyret C, Durand C, Selmi-Ruby S, Giroud H, Berger-Dutrieux N, et al. Silencing of the tumor suppressor gene SLC5A8 is associated with BRAF mutations in classical papillary thyroid carcinomas. *The Journal of clinical endocrinology and metabolism* 2005;90(5):3028-35.

41. Camerino DC, Tricarico D, Desaphy JF. Ion channel pharmacology. *Neurotherapeutics : the journal of the American Society for Experimental NeuroTherapeutics* 2007;4(2):184-98.
42. Urrego D, Tomczak AP, Zahed F, Stuhmer W, Pardo LA. Potassium channels in cell cycle and cell proliferation. *Philosophical transactions of the Royal Society of London Series B, Biological sciences* 2014;369(1638):20130094.
43. Yost CS. Potassium channels: basic aspects, functional roles, and medical significance. *Anesthesiology* 1999;90(4):1186-203.
44. Warmke JW, Ganetzky B. A family of potassium channel genes related to eag in *Drosophila* and mammals. *Proceedings of the National Academy of Sciences of the United States of America* 1994;91(8):3438-42.
45. Wymore RS, Gintant GA, Wymore RT, Dixon JE, McKinnon D, Cohen IS. Tissue and species distribution of mRNA for the IKr-like K<sup>+</sup> channel, erg. *Circulation research* 1997;80(2):261-8.
46. Shieh CC, Coghlan M, Sullivan JP, Gopalakrishnan M. Potassium channels: molecular defects, diseases, and therapeutic opportunities. *Pharmacological reviews* 2000;52(4):557-94.
47. Vandenberg JI, Perry MD, Perrin MJ, Mann SA, Ke Y, Hill AP. hERG K(+) channels: structure, function, and clinical significance. *Physiological reviews* 2012;92(3):1393-478.
48. Zhou PZ, Babcock J, Liu LQ, Li M, Gao ZB. Activation of human ether-a-go-go related gene (hERG) potassium channels by small molecules. *Acta pharmacologica Sinica* 2011;32(6):781-8.
49. Morais Cabral JH, Lee A, Cohen SL, Chait BT, Li M, Mackinnon R. Crystal structure and functional analysis of the HERG potassium channel N terminus: a eukaryotic PAS domain. *Cell* 1998;95(5):649-55.
50. Perrin MJ, Subbiah RN, Vandenberg JI, Hill AP. Human ether-a-go-go related gene (hERG) K<sup>+</sup> channels: function and dysfunction. *Progress in biophysics and molecular biology* 2008;98(2-3):137-48.
51. Vandenberg JI, Torres AM, Campbell TJ, Kuchel PW. The HERG K<sup>+</sup> channel: progress in understanding the molecular basis of its unusual gating kinetics. *European biophysics journal : EBJ* 2004;33(2):89-97.
52. Sanguinetti MC, Tristani-Firouzi M. hERG potassium channels and cardiac arrhythmia. *Nature* 2006;440(7083):463-9.
53. Tester DJ, Ackerman MJ. Cardiomyopathic and channelopathic causes of sudden unexplained death in infants and children. *Annual review of medicine* 2009;60:69-84.
54. Sanguinetti MC. HERG1 channelopathies. *Pflugers Archiv : European journal of physiology* 2010;460(2):265-76.
55. Wulff H, Castle NA, Pardo LA. Voltage-gated potassium channels as therapeutic targets. *Nature reviews Drug discovery* 2009;8(12):982-1001.

56. Brugada R, Hong K, Dumaine R, Cordeiro J, Gaita F, Borggrefe M, et al. Sudden death associated with short-QT syndrome linked to mutations in HERG. *Circulation* 2004;109(1):30-5.
57. Sun Y, Quan XQ, Fromme S, Cox RH, Zhang P, Zhang L, et al. A novel mutation in the KCNH2 gene associated with short QT syndrome. *Journal of molecular and cellular cardiology* 2011;50(3):433-41.
58. Itoh H, Sakaguchi T, Ashihara T, Ding WG, Nagaoka I, Oka Y, et al. A novel KCNH2 mutation as a modifier for short QT interval. *International journal of cardiology* 2009;137(1):83-5.
59. Algra A, Tijssen JG, Roelandt JR, Pool J, Lubsen J. Heart rate variability from 24-hour electrocardiography and the 2-year risk for sudden death. *Circulation* 1993;88(1):180-5.
60. Gaita F, Giustetto C, Bianchi F, Schimpf R, Haissaguerre M, Calo L, et al. Short QT syndrome: pharmacological treatment. *Journal of the American College of Cardiology* 2004;43(8):1494-9.
61. Parkington HC, Stevenson J, Tonta MA, Paul J, Butler T, Maiti K, et al. Diminished hERG K<sup>+</sup> channel activity facilitates strong human labour contractions but is dysregulated in obese women. *Nature communications* 2014;5:4108.
62. Omichi C, Momose Y, Kitahara S. Congenital long QT syndrome presenting with a history of epilepsy: misdiagnosis or relationship between channelopathies of the heart and brain? *Epilepsia* 2010;51(2):289-92.
63. Teng GQ, Zhao X, Lees-Miller JP, Quinn FR, Li P, Rancourt DE, et al. Homozygous missense N629D hERG (KCNH2) potassium channel mutation causes developmental defects in the right ventricle and its outflow tract and embryonic lethality. *Circulation research* 2008;103(12):1483-91.
64. Arcangeli A, Rosati B, Crociani O, Cherubini A, Fontana L, Passani B, et al. Modulation of HERG current and herg gene expression during retinoic acid treatment of human neuroblastoma cells: potentiating effects of BDNF. *Journal of neurobiology* 1999;40(2):214-25.
65. Bianchi L, Wible B, Arcangeli A, Tagliatela M, Morra F, Castaldo P, et al. herg encodes a K<sup>+</sup> current highly conserved in tumors of different histogenesis: a selective advantage for cancer cells? *Cancer research* 1998;58(4):815-22.
66. Meves H, Schwarz JR, Wulfsen I. Separation of M-like current and ERG current in NG108-15 cells. *British journal of pharmacology* 1999;127(5):1213-23.
67. Smith GA, Tsui HW, Newell EW, Jiang X, Zhu XP, Tsui FW, et al. Functional up-regulation of HERG K<sup>+</sup> channels in neoplastic hematopoietic cells. *The Journal of biological chemistry* 2002;277(21):18528-34.

68. Crociani O, Guasti L, Balzi M, Becchetti A, Wanke E, Olivotto M, et al. Cell cycle-dependent expression of HERG1 and HERG1B isoforms in tumor cells. *The Journal of biological chemistry* 2003;278(5):2947-55.
69. Lastraioli E, Guasti L, Crociani O, Polvani S, Hofmann G, Witchel H, et al. herg1 gene and HERG1 protein are overexpressed in colorectal cancers and regulate cell invasion of tumor cells. *Cancer research* 2004;64(2):606-11.
70. Jehle J, Schweizer PA, Katus HA, Thomas D. Novel roles for hERG K(+) channels in cell proliferation and apoptosis. *Cell death & disease* 2011;2:e193.
71. Curran ME, Splawski I, Timothy KW, Vincent GM, Green ED, Keating MT. A molecular basis for cardiac arrhythmia: HERG mutations cause long QT syndrome. *Cell* 1995;80(5):795-803.
72. Wright EM, Turk E. The sodium/glucose cotransport family SLC5. *Pflugers Archiv : European journal of physiology* 2004;447(5):510-8.
73. Wright EM, Loo DD, Hirayama BA, Turk E. Surprising versatility of Na<sup>+</sup>-glucose cotransporters: SLC5. *Physiology* 2004;19:370-6.
74. Zhou L, Cryan EV, D'Andrea MR, Belkowski S, Conway BR, Demarest KT. Human cardiomyocytes express high level of Na<sup>+</sup>/glucose cotransporter 1 (SGLT1). *Journal of cellular biochemistry* 2003;90(2):339-46.
75. Sabino-Silva R, Freitas HS, Lamers ML, Okamoto MM, Santos MF, Machado UF. Na<sup>+</sup>-glucose cotransporter SGLT1 protein in salivary glands: potential involvement in the diabetes-induced decrease in salivary flow. *The Journal of membrane biology* 2009;228(2):63-9.
76. Wright EM, Hirayama BA, Loo DF. Active sugar transport in health and disease. *Journal of internal medicine* 2007;261(1):32-43.
77. Turk E, Zabel B, Mundlos S, Dyer J, Wright EM. Glucose/galactose malabsorption caused by a defect in the Na<sup>+</sup>/glucose cotransporter. *Nature* 1991;350(6316):354-6.
78. Casneuf VF, Fonteyne P, Van Damme N, Demetter P, Pauwels P, de Hemptinne B, et al. Expression of SGLT1, Bcl-2 and p53 in primary pancreatic cancer related to survival. *Cancer investigation* 2008;26(8):852-9.
79. Engelman JA, Cantley LC. A sweet new role for EGFR in cancer. *Cancer cell* 2008;13(5):375-6.
80. Ganapathy V, Thangaraju M, Prasad PD. Nutrient transporters in cancer: relevance to Warburg hypothesis and beyond. *Pharmacology & therapeutics* 2009;121(1):29-40.
81. Weihua Z, Tsan R, Huang WC, Wu Q, Chiu CH, Fidler IJ, et al. Survival of cancer cells is maintained by EGFR independent of its kinase activity. *Cancer cell* 2008;13(5):385-93.

82. Biber J, Hernando N, Forster I. Phosphate transporters and their function. *Annual review of physiology* 2013;75:535-50.
83. Marks J, Debnam ES, Unwin RJ. Phosphate homeostasis and the renal-gastrointestinal axis. *American journal of physiology Renal physiology* 2010;299(2):F285-96.
84. Virkki LV, Biber J, Murer H, Forster IC. Phosphate transporters: a tale of two solute carrier families. *American journal of physiology Renal physiology* 2007;293(3):F643-54.
85. Mulroney SE, Woda CB, Halaihel N, Louie B, McDonnell K, Schulkin J, et al. Central control of renal sodium-phosphate (NaPi-2) transporters. *American journal of physiology Renal physiology* 2004;286(4):F647-52.
86. Lundquist P, Murer H, Biber J. Type II Na<sup>+</sup>-Pi cotransporters in osteoblast mineral formation: regulation by inorganic phosphate. *Cellular physiology and biochemistry : international journal of experimental cellular physiology, biochemistry, and pharmacology* 2007;19(1-4):43-56.
87. Khadeer MA, Tang Z, Tenenhouse HS, Eiden MV, Murer H, Hernando N, et al. Na<sup>+</sup>-dependent phosphate transporters in the murine osteoclast: cellular distribution and protein interactions. *American journal of physiology Cell physiology* 2003;284(6):C1633-44.
88. Forster IC, Kohler K, Biber J, Murer H. Forging the link between structure and function of electrogenic cotransporters: the renal type IIa Na<sup>+</sup>/Pi cotransporter as a case study. *Progress in biophysics and molecular biology* 2002;80(3):69-108.
89. Forster IC, Hernando N, Biber J, Murer H. Proximal tubular handling of phosphate: A molecular perspective. *Kidney international* 2006;70(9):1548-59.
90. Gisler SM, Kittanakom S, Fuster D, Wong V, Bertic M, Radanovic T, et al. Monitoring protein-protein interactions between the mammalian integral membrane transporters and PDZ-interacting partners using a modified split-ubiquitin membrane yeast two-hybrid system. *Molecular & cellular proteomics : MCP* 2008;7(7):1362-77.
91. Wagner CA, Hernando N, Forster IC, Biber J. The SLC34 family of sodium-dependent phosphate transporters. *Pflugers Archiv : European journal of physiology* 2014;466(1):139-53.
92. Tenenhouse HS. Regulation of phosphorus homeostasis by the type IIa Na<sup>+</sup>/phosphate cotransporter. *Annual review of nutrition* 2005;25:197-214.
93. Beck L, Karaplis AC, Amizuka N, Hewson AS, Ozawa H, Tenenhouse HS. Targeted inactivation of Npt2 in mice leads to severe renal phosphate wasting, hypercalciuria, and skeletal abnormalities. *Proceedings of the National Academy of Sciences of the United States of America* 1998;95(9):5372-7.
94. Hilfiker H, Hattenhauer O, Traebert M, Forster I, Murer H, Biber J. Characterization of a murine type II sodium-phosphate cotransporter

- expressed in mammalian small intestine. *Proceedings of the National Academy of Sciences of the United States of America* 1998;95(24):14564-9.
95. Radanovic T, Wagner CA, Murer H, Biber J. Regulation of intestinal phosphate transport. I. Segmental expression and adaptation to low-P(i) diet of the type IIb Na(+)-P(i) cotransporter in mouse small intestine. *American journal of physiology Gastrointestinal and liver physiology* 2005;288(3):G496-500.
  96. Xu Y, Yeung CH, Setiawan I, Avram C, Biber J, Wagenfeld A, et al. Sodium-inorganic phosphate cotransporter NaPi-IIb in the epididymis and its potential role in male fertility studied in a transgenic mouse model. *Biology of reproduction* 2003;69(4):1135-41.
  97. Frei P, Gao B, Hagenbuch B, Mate A, Biber J, Murer H, et al. Identification and localization of sodium-phosphate cotransporters in hepatocytes and cholangiocytes of rat liver. *American journal of physiology Gastrointestinal and liver physiology* 2005;288(4):G771-8.
  98. Miyoshi K, Shillingford JM, Smith GH, Grimm SL, Wagner KU, Oka T, et al. Signal transducer and activator of transcription (Stat) 5 controls the proliferation and differentiation of mammary alveolar epithelium. *The Journal of cell biology* 2001;155(4):531-42.
  99. Homann V, Rosin-Steiner S, Stratmann T, Arnold WH, Gaengler P, Kinne RK. Sodium-phosphate cotransporter in human salivary glands: molecular evidence for the involvement of NPT2b in acinar phosphate secretion and ductal phosphate reabsorption. *Archives of oral biology* 2005;50(9):759-68.
  100. Yin BW, Kiyamova R, Chua R, Caballero OL, Gout I, Gryshkova V, et al. Monoclonal antibody MX35 detects the membrane transporter NaPi2b (SLC34A2) in human carcinomas. *Cancer immunity* 2008;8:3.
  101. Ferreira Francisco FA, Pereira e Silva JL, Hochegger B, Zanetti G, Marchiori E. Pulmonary alveolar microlithiasis. State-of-the-art review. *Respiratory medicine* 2013;107(1):1-9.
  102. Kim B, Winter TC, 3rd, Ryu JA. Testicular microlithiasis: clinical significance and review of the literature. *European radiology* 2003;13(12):2567-76.
  103. Rangel LB, Sherman-Baust CA, Wernyj RP, Schwartz DR, Cho KR, Morin PJ. Characterization of novel human ovarian cancer-specific transcripts (HOSTs) identified by serial analysis of gene expression. *Oncogene* 2003;22(46):7225-32.
  104. Jarzab B, Wiench M, Fujarewicz K, Simek K, Jarzab M, Oczko-Wojciechowska M, et al. Gene expression profile of papillary thyroid cancer: sources of variability and diagnostic implications. *Cancer research* 2005;65(4):1587-97.

105. Chen DR, Chien SY, Kuo SJ, Teng YH, Tsai HT, Kuo JH, et al. SLC34A2 as a novel marker for diagnosis and targeted therapy of breast cancer. *Anticancer research* 2010;30(10):4135-40.
106. Orton RJ, Sturm OE, Vyshemirsky V, Calder M, Gilbert DR, Kolch W. Computational modelling of the receptor-tyrosine-kinase-activated MAPK pathway. *The Biochemical journal* 2005;392(Pt 2):249-61.
107. Pakladok T, Hosseinzadeh Z, Alesutan I, Lang F. Stimulation of the Na(+)-coupled glucose transporter SGLT1 by B-RAF. *Biochemical and biophysical research communications* 2012;427(4):689-93.
108. Huang FD, Chen J, Lin M, Keating MT, Sanguinetti MC. Long-QT syndrome-associated missense mutations in the pore helix of the HERG potassium channel. *Circulation* 2001;104(9):1071-5.
109. Hediger MA, Turk E, Wright EM. Homology of the human intestinal Na<sup>+</sup>/glucose and Escherichia coli Na<sup>+</sup>/proline cotransporters. *Proceedings of the National Academy of Sciences of the United States of America* 1989;86(15):5748-52.
110. Bhandaru M, Kempe DS, Rotte A, Capuano P, Pathare G, Sopjani M, et al. Decreased bone density and increased phosphaturia in gene-targeted mice lacking functional serum- and glucocorticoid-inducible kinase 3. *Kidney international* 2011;80(1):61-7.
111. Guan B, Chen X, Zhang H. Two-electrode voltage clamp. *Methods in molecular biology* 2013;998:79-89.
112. Hamill OP, Marty A, Neher E, Sakmann B, Sigworth FJ. Improved patch-clamp techniques for high-resolution current recording from cells and cell-free membrane patches. *Pflugers Archiv : European journal of physiology* 1981;391(2):85-100.
113. Barry PH, Lynch JW. Liquid junction potentials and small cell effects in patch-clamp analysis. *The Journal of membrane biology* 1991;121(2):101-17.
114. Almilaji A, Munoz C, Elvira B, Fajol A, Pakladok T, Honisch S, et al. AMP-activated protein kinase regulates hERG potassium channel. *Pflugers Archiv : European journal of physiology* 2013; in press.
115. Pakladok T, Hosseinzadeh Z, Almilaji A, Lebedeva A, Shumilina E, Alesutan I, et al. Up-regulation of hERG K(+) channels by B-RAF. *PloS one* 2014;9(1):e87457.
116. Lamothe SM, Zhang S. The serum- and glucocorticoid-inducible kinases SGK1 and SGK3 regulate hERG channel expression via ubiquitin ligase Nedd4-2 and GTPase Rab11. *The Journal of biological chemistry* 2013;288(21):15075-84.
117. Wang T, Hogan-Cann A, Kang Y, Cui Z, Guo J, Yang T, et al. Muscarinic receptor activation increases hERG channel expression through phosphorylation of ubiquitin ligase Nedd4-2. *Molecular pharmacology* 2014;85(6):877-86.



118. Guo J, Wang T, Li X, Shallow H, Yang T, Li W, et al. Cell surface expression of human ether-a-go-go-related gene (hERG) channels is regulated by caveolin-3 protein via the ubiquitin ligase Nedd4-2. *The Journal of biological chemistry* 2012;287(40):33132-41.
119. Zhang DY, Wang Y, Lau CP, Tse HF, Li GR. Both EGFR kinase and Src-related tyrosine kinases regulate human ether-a-go-go-related gene potassium channels. *Cellular signalling* 2008;20(10):1815-21.
120. Sisko JT, Tucker TJ, Bilodeau MT, Buser CA, Cieccko PA, Coll KE, et al. Potent 2-[(pyrimidin-4-yl)amine]-1,3-thiazole-5-carbonitrile-based inhibitors of VEGFR-2 (KDR) kinase. *Bioorganic & medicinal chemistry letters* 2006;16(5):1146-50.
121. Maier G, Palmada M, Rajamanickam J, Shumilina E, Bohmer C, Lang F. Upregulation of HERG channels by the serum and glucocorticoid inducible kinase isoform SGK3. *Cellular physiology and biochemistry : international journal of experimental cellular physiology, biochemistry, and pharmacology* 2006;18(4-5):177-86.
122. Pakladok T, Almilaji A, Munoz C, Alesutan I, Lang F. PIKfyve sensitivity of hERG channels. *Cellular physiology and biochemistry : international journal of experimental cellular physiology, biochemistry, and pharmacology* 2013;31(6):785-94.
123. Ouadid-Ahidouch H, Ahidouch A. K(+) channels and cell cycle progression in tumor cells. *Frontiers in physiology* 2013;4:220.
124. Glassmeier G, Hempel K, Wulfsen I, Bauer CK, Schumacher U, Schwarz JR. Inhibition of HERG1 K<sup>+</sup> channel protein expression decreases cell proliferation of human small cell lung cancer cells. *Pflugers Archiv : European journal of physiology* 2012;463(2):365-76.
125. Arcangeli A. Expression and role of hERG channels in cancer cells. *Novartis Foundation symposium* 2005;266:225-32; discussion 32-4.
126. Asher V, Sowter H, Shaw R, Bali A, Khan R. Eag and HERG potassium channels as novel therapeutic targets in cancer. *World J Surg Oncol* 2010;8:113.
127. Pillozzi S, Arcangeli A. Physical and functional interaction between integrins and hERG1 channels in cancer cells. *Adv Exp Med Biol* 2010;674:55-67.
128. Thomas D, Karle CA, Kiehn J. The cardiac hERG/IKr potassium channel as pharmacological target: structure, function, regulation, and clinical applications. *Current pharmaceutical design* 2006;12(18):2271-83.
129. Muslin AJ. Role of raf proteins in cardiac hypertrophy and cardiomyocyte survival. *Trends in cardiovascular medicine* 2005;15(6):225-9.
130. Kramann N, Hasenfuss G, Seidler T. B-RAF and its novel negative regulator reticulocalbin 1 (RCN1) modulates cardiomyocyte hypertrophy. *Cardiovascular research* 2014;102(1):88-96.

131. Cheng H, Kari G, Dicker AP, Rodeck U, Koch WJ, Force T. A novel preclinical strategy for identifying cardiotoxic kinase inhibitors and mechanisms of cardiotoxicity. *Circulation research* 2011;109(12):1401-9.
132. Hirsch JR, Loo DD, Wright EM. Regulation of Na<sup>+</sup>/glucose cotransporter expression by protein kinases in *Xenopus laevis* oocytes. *The Journal of biological chemistry* 1996;271(25):14740-6.
133. Subramanian S, Glitz P, Kipp H, Kinne RK, Castaneda F. Protein kinase-A affects sorting and conformation of the sodium-dependent glucose co-transporter SGLT1. *Journal of cellular biochemistry* 2009;106(3):444-52.
134. Castaneda-Sceppa C, Subramanian S, Castaneda F. Protein kinase C mediated intracellular signaling pathways are involved in the regulation of sodium-dependent glucose co-transporter SGLT1 activity. *Journal of cellular biochemistry* 2010;109(6):1109-17.
135. Dieter M, Palmada M, Rajamanickam J, Aydin A, Busjahn A, Boehmer C, et al. Regulation of glucose transporter SGLT1 by ubiquitin ligase Nedd4-2 and kinases SGK1, SGK3, and PKB. *Obesity research* 2004;12(5):862-70.
136. Sopjani M, Bhavsar SK, Fraser S, Kemp BE, Foller M, Lang F. Regulation of Na<sup>+</sup>-coupled glucose carrier SGLT1 by AMP-activated protein kinase. *Molecular membrane biology* 2010;27(2-3):137-44.
137. Hosseinzadeh Z, Bhavsar SK, Shojaiefard M, Saxena A, Merches K, Sopjani M, et al. Stimulation of the glucose carrier SGLT1 by JAK2. *Biochemical and biophysical research communications* 2011;408(2):208-13.
138. Ishikawa N, Oguri T, Isobe T, Fujitaka K, Kohno N. SGLT gene expression in primary lung cancers and their metastatic lesions. *Japanese journal of cancer research : Gann* 2001;92(8):874-9.
139. Matosin-Matekalo M, Mesonero JE, Delezay O, Poiree JC, Ilundain AA, Brot-Laroche E. Thyroid hormone regulation of the Na<sup>+</sup>/glucose cotransporter SGLT1 in Caco-2 cells. *The Biochemical journal* 1998;334 ( Pt 3):633-40.
140. Mendez LE, Mancini N, Cantuaria G, Gomez-Marin O, Penalver M, Braunschweiger P, et al. Expression of glucose transporter-1 in cervical cancer and its precursors. *Gynecologic oncology* 2002;86(2):138-43.
141. Rudlowski C, Becker AJ, Schroder W, Rath W, Buttner R, Moser M. GLUT1 messenger RNA and protein induction relates to the malignant transformation of cervical cancer. *American journal of clinical pathology* 2003;120(5):691-8.
142. Lang F, Busch GL, Ritter M, Volkl H, Waldegger S, Gulbins E, et al. Functional significance of cell volume regulatory mechanisms. *Physiological reviews* 1998;78(1):247-306.
143. Pakladok T, Hosseinzadeh Z, Lebedeva A, Alesutan I, Lang F. Upregulation of the Na<sup>(+)</sup>-coupled phosphate cotransporters NaPi-IIa and NaPi-IIb by B-RAF. *The Journal of membrane biology* 2014;247(2):137-45.

144. Wallace DP. Cyclic AMP-mediated cyst expansion. *Biochimica et biophysica acta* 2011;1812(10):1291-300.
145. Ishiki M, Klip A. Minireview: recent developments in the regulation of glucose transporter-4 traffic: new signals, locations, and partners. *Endocrinology* 2005;146(12):5071-8.
146. Whiteman EL, Cho H, Birnbaum MJ. Role of Akt/protein kinase B in metabolism. *Trends in endocrinology and metabolism: TEM* 2002;13(10):444-51.
147. Carranza A, Musolino PL, Villar M, Nowicki S. Signaling cascade of insulin-induced stimulation of L-dopa uptake in renal proximal tubule cells. *American journal of physiology Cell physiology* 2008;295(6):C1602-9.
148. Green CJ, Goransson O, Kular GS, Leslie NR, Gray A, Alessi DR, et al. Use of Akt inhibitor and a drug-resistant mutant validates a critical role for protein kinase B/Akt in the insulin-dependent regulation of glucose and system A amino acid uptake. *The Journal of biological chemistry* 2008;283(41):27653-67.
149. Vaughan-Jones RD, Swietach P. Pushing and pulling the cardiac sodium/hydrogen exchanger. *Circulation research* 2008;103(8):773-5.
150. Lee IH, Dinudom A, Sanchez-Perez A, Kumar S, Cook DI. Akt mediates the effect of insulin on epithelial sodium channels by inhibiting Nedd4-2. *The Journal of biological chemistry* 2007;282(41):29866-73.
151. Foller M, Kempe DS, Boini KM, Pathare G, Siraskar B, Capuano P, et al. PKB/SGK-resistant GSK3 enhances phosphaturia and calciuria. *Journal of the American Society of Nephrology : JASN* 2011;22(5):873-80.
152. Kempe DS, Ackermann TF, Boini KM, Klaus F, Umbach AT, Dermaku-Sopjani M, et al. Akt2/PKBbeta-sensitive regulation of renal phosphate transport. *Acta physiologica* 2010;200(1):75-85.
153. Guan KL, Figueroa C, Brtva TR, Zhu T, Taylor J, Barber TD, et al. Negative regulation of the serine/threonine kinase B-Raf by Akt. *The Journal of biological chemistry* 2000;275(35):27354-9.
154. Zhang BH, Tang ED, Zhu T, Greenberg ME, Vojtek AB, Guan KL. Serum- and glucocorticoid-inducible kinase SGK phosphorylates and negatively regulates B-Raf. *The Journal of biological chemistry* 2001;276(34):31620-6.

## 7 Contribution

This thesis includes the data of the three following original papers.

In publication 1 (Pakladok et al., 2014), LF and SE designed the concept of the work. I performed immunostaining, confocal microscopy and chemiluminescence experiments in *Xenopus* oocytes, maintained the RD cells in culture, made the treatments (Fig.13 A, B and Fig.15). I also carried out the surface biotinylation experiments and western blotting in RD cells (Fig.16 A, B). LA accomplished the flow cytometry measurements (Fig.17 A, B). AA performed patch clamp experiments under the supervision of SE (Fig.18 A-C). HZ carried out the handling and injection of *Xenopus* oocytes as well as two-electrode voltage clamp recordings (Fig.11-12 A, B and Fig.14 A, B). The statistical analysis was performed by me under supervision of AI and SE. LF wrote the draft. I revised and completed the paper with the help of AI. All the authors read and approved the manuscript.

In publication 2 (Pakladok et al., 2012), LF and AI set up the concept of the work. I performed the chemiluminescence and immunofluorescence experiments in *Xenopus* oocytes (Fig.21 A, B). HZ carried out the voltage clamp experiments (Fig.19 A, B and Fig.20). The statistical analysis was accomplished by me with the help of AI. LF wrote the draft. I revised and completed the paper under supervision of AI.

In publication 3 (Pakladok et al., 2014), I contributed to the layout of the study in cooperation with LF and AI. I performed immunostaining, confocal microscopy and chemiluminescence experiments in *Xenopus* oocytes (Fig.24 A, B). Further I maintained HEK293 cells in culture. I performed biotinylation of the cell surface proteins and western blot experiments (Fig.25 A, B). HZ carried out the voltage clamp experiments (Fig. 22 A, B; Fig.23; Fig.26 A, B and Fig.27). LA helped with data interpretation. The statistical analysis was accomplished by me with the help of AI. LF wrote the draft. I revised and completed the paper under supervision of AI.

I hereby declare that this thesis is my own work and effort and that it has not been submitted anywhere else for any award. Other sources are acknowledged and a reference is appended.

## 8 Original papers

1. Pakladok T, Hosseinzadeh Z, Almilaji A, Lebedeva A, Shumilina E, Alesutan I, Lang F. Up-regulation of hERG K<sup>+</sup> channels by B-RAF. PLoS One. 2014 Jan 27; 9(1):e87457.
2. Pakladok T, Hosseinzadeh Z, Alesutan I, Lang F. Stimulation of the Na(+)-coupled glucose transporter SGLT1 by B-RAF. Biochem Biophys Res Commun. 2012 Nov 2; 427(4):689-93.
3. Pakladok T, Hosseinzadeh Z, Lebedeva A, Alesutan I, Lang F. Upregulation of the Na<sup>+</sup>-coupled phosphate cotransporters NaPi-IIa and NaPi-IIb by B-RAF. J Membr Biol. 2014 Feb; 247(2):137-45.

## 9 Acknowledgments

I am using this opportunity to express my gratitude to everyone who supported me throughout my PhD. I am thankful for their guidance, constructive criticism and friendly advice during my work.

I would like to express my special appreciation and thanks to my supervisor Professor Dr. Florian Lang for giving me the opportunity to carry out my dissertation in his department. I want to thank him for encouraging my research and for allowing me to grow as a researcher.

I would also like to thank my group leader Dr. Ioana Alesutan for her professional attitude and practical guidance. I am thankful to her for the time and efforts she has spent to help me to finalize my thesis.

I am grateful to Dr. Jakob Völkl for his tremendous help and the much needed assistance and support.

I thank my colleagues Zohreh Hosseinzadeh, Aleksandra Lebedeva, Ahmad Almilaji and Ekaterina Shumilina for their enthusiasm, intensity and eagerness to cooperate.

I am thankful to all the members of the Physiology I who helped me in the one way or the other to finish my work successfully. I am grateful to the technical staff of the department, especially Elfriede Faber, Uwe Schüller, Lejla Subasic, Jan Wiech, Tanja Loch and Sari Rube for their kind assistance and help.

A special thanks to my parents for their unconditional support through everything I did and do. I would also like to thank my sister and her husband for being a constant source of inspiration and encouragement. My warm thanks to my brother and his wife, you know how important you are to me.

Finally, I would like to thank my husband for his faith in me and support whenever I needed it the most.

## 10 Curriculum Vitae

### Persönliche Angaben

---

Vor- und Zuname Tatsiana Castor (geb. Pakladok)

Geburtsdatum 24.01.1986

Staatsangehörigkeit weißrussisch

### Berufserfahrung

---

04/2011 - dato **Doktorandin zur Erlangung des Doktorgrades der Humanwissenschaften (Dr. sc. hum.)**, Medizinische Fakultät, Physiologie I, Eberhard Karls Universität Tübingen

- Durchführen molekular-biologischer Experimente: Zellkultur, Westernblot, Immunzytochemie und Konfokalmikroskopie, Chemilumineszenzanalyse
- Zusammenarbeit mit Forschungsgruppen innerhalb und außerhalb der Universität (in internationalen Teams)

09/2009 - 04/2011 **Doktorandin**, Technische Universität des Nahen Ostens, Graduate School of Natural and Applied Sciences, Ankara, Türkei

- Mitarbeit in der Arbeitsgruppe Neuroendokrinologie
- Weiterbildung auf den Gebieten: Neuroendokrinologie, Biotechnologie, Molekulare Krebsbiologie und Biowerkstoffe

08/2008 - 09/2009 **Wissenschaftliche Mitarbeiterin**, Institut für Genetik und Zytologie, Akademie der Wissenschaften, Minsk, Weißrussland

## Ausbildung

---

- 09/2003 - 06/2008     **Diplom Biologin** (Gesamtnote „sehr gut“, mit Auszeichnung)  
**Studium des Medizin- und Biologiewesens**  
Sacharow Internationale Staatliche Universität für Ökologie, Minsk, Weißrussland  
– Schwerpunkte: Biochemie, Physiologie, Molekularbiologie, Mikrobiologie  
  
Titel der Diplomarbeit: *„Die Häufigkeit von polymorphen Allelen des Insulingenes in der Population von Belarussen“* (Note „sehr gut“)
- 09/1993 - 06/2003     **Allgemeine Hochschulreife**, Abschlussnote „sehr gut“  
Mittelschule in Molodetschno, Weißrussland